
Remote sensing of the Sacramento-San Joaquin Delta to
enhance mapping for invasive and native aquatic plant
species

December 2021

Funding Agreement:

Delta Stewardship Council (#DSC-20024)

Submitted by: Susan L. Ustin (Principal Investigator)

Contributions by: Shruti Khanna and Mui Lay



CENTER FOR SPATIAL TECHNOLOGIES
AND REMOTE SENSING
DEPT. OF LAND, AIR AND WATER RESOURCES



Table of Contents

1.	Executive Summary	1
2.	Introduction	2
3.	Study Area Description	3
3.1	<i>Habitat</i>	3
3.2	<i>Aquatic Plant Communities</i>	4
4.	Image Acquisition and Pre-processing	5
5.	Field Data Collection	9
6.	Image Classification	12
6.1	<i>Data Reduction Techniques</i>	12
6.2	<i>Classifier</i>	15
7.	Results	16
7.1	<i>Accuracy Assessment</i>	16
7.2	<i>Acreage Calculations</i>	20
8.	Key Questions to be Addressed	25
8.1	<i>Ideal Window for Image Acquisition</i>	25
8.2	<i>Comparing the Monitoring Scenarios</i>	25
8.3	<i>Evaluation of Changing DBW Treatment Plans</i>	26
8.4	<i>Google Earth Engine Applications for Sentinel Project</i>	26
9.	Site Maps	27
9.1	<i>Sherman Lake</i>	27
9.2	<i>Big Break</i>	29
9.3	<i>Liberty Island</i>	30
9.4	<i>Frank's Tract</i>	32
9.5	<i>Rhode Island</i>	33
9.6	<i>Venice Cut</i>	34
9.7	<i>Ward Cut</i>	35
10.	References	37
11.	Appendix A. Classifier inputs and their description	41

1. Executive Summary

The Sacramento-San Joaquin Delta (henceforth, Delta) is an area of 2,219 Km² with about 1,800 Km waterways. It provides drinking water for more than 23 million people while supporting a multi-billion dollar agricultural industry and an extensive recreational boating and fishing industry. Starting in the late 1980s major invasive aquatic plants began to expand their distributions, the most aggressive of which are *Pontederia crassipes* (water hyacinth), *Ludwigia* spp. (water primrose) and *Egeria densa* (Brazilian waterweed). Containment methods began in the late 1990s and still continue today. The extent of these species has expanded in recent years with the 2011-2015 drought.

Mapping of invasive species in the Delta has been sporadic since 2003, when we first began. The current project, to map the status of invasive species by acquiring imagery in Summer 2020 and analyzing it was funded for two main purposes – 1) to ensure that the time series of invasive species mapping continued and 2) to determine seasonal and annual impacts of herbicide management of invasive species.

SpecTIR LLC from Reno, NV, flew their Fenix 1K hyperspectral imager over the Delta on dates between July 15 -18, 2020. The Fenix sensor measures 348 spectral bands across the visible and near-infrared spectrum (380-970nm) and 274 spectral bands in the Shortwave infrared spectrum (970nm- 2500nm), at a nominal spatial resolution of 2x2m.

Field data of aquatic species were collected by boats provided by California Department of Food and Agriculture (CDFA) and staffed with Center for Spatial Technologies And Remote Sensing (CSTARS) and CDFA personnel between July 20-31, 2020. These data were used for training and validation of the remotely sensed images. The crews collected 838 points for the dominant submerged (SAV), floating (FAV), and emergent (EAV) vegetation species in the Delta. For each point they noted attributes such as species name(s), location, cover estimates, patch size and azimuthal orientation in the long direction. In addition, rake data and Secchi depth were measured at SAV points.

The Random Forests (RF) machine learning algorithm was used to classify the imagery. The resulting classification was highly consistent with the field data, producing pixel-based overall accuracy of 90.4% with a kappa value of 0.89 (indicating excellent agreement) for the Delta. All species-specific accuracies in the Delta were > 80% except for Phragmites and Arundo classes which had the lowest accuracies. In the legal Delta, in Summer 2020, SAV covered 3776 ha or 23.2% of waterways, water primrose covered 514 ha and water hyacinth covered 232 ha, collectively occupying 4.6% of waterways.

2. Introduction

The Sacramento-San Joaquin River Delta is recognized to be one of the most invaded estuaries in the world (Cohen and Carlton, 1998). The hydrology of the Delta has undergone extensive alteration with its system of levees and dams in concert with massive upriver federal and state reclamation projects. Currently managed as a tidal freshwater system, it supplies valuable water resources more than 23 million people, supports a multibillion dollar agricultural industry and 14.4 million person-days of recreational boating and 11.8 million person-days of recreational fishing (these are not combined because of likely over-counting; www.ca.gov/rec_eco_recreation.htm). In recent decades eutrophication has increased significantly (Nichols et al., 1986), while suspended sediment inputs and turbidity have declined (Hestir, 2010; Wright and Schoellhamer, 2004). The altered hydrology of the Delta has made its ecosystem susceptible to invasion by eliminating the competitive advantage of low-nutrient-brackish-adapted native species (Bossard et al., 2000; Cook, 1990; Sculthorpe, 1967) while providing enough nutrients (Bicudo et al., 2007) and reduced salinity for opportunistic species to become competitive. In particular, three aggressive freshwater invasive plants that flourish in high-nutrient conditions but are ill-adapted to high salinity (Cook and Urmi-König, 1984; El-Gendy et al., 2005; Gopal, 1987; Penfound and Earle, 1948) have established in the Delta: the Floating Aquatic Vegetation (FAV) species, *Pontederia crassipes* (water hyacinth) and *Ludwigia* (water primrose) and the Submerged Aquatic Vegetation (SAV) species, *Egeria densa* (Brazilian waterweed).

Once invasive species are well-established in a degraded ecosystem, they promote an alternative ecosystem state that is resistant to further change due to positive feedback loops (Scheffer et al., 2007). For example, the process of eutrophication spurs the growth of macrophytic FAV which is usually limited by nutrients in the water column (Scheffer et al., 2003). As the FAV canopy expands, it shades macrophytic SAV, thus concurrently reducing SAV cover. Decomposing plant matter below the floating mats creates anoxic conditions, mobilizing phosphorus and other nutrients in the sediment, furthering nutrient loading which continues to inhibit reestablishment of SAV (Scheffer et al., 2007). Alternatively, under conditions that favor SAV, once it is established, SAV can slow water velocity by over 40-80% (Lacy et al., 2021; Wilcock et al., 1999), which decreases sediment re-suspension. This in turn increases light availability through the water column, and slows water column nutrient recycling rates (Horppila and Nurminen, 2003; Koch, 2001), creating conditions more favorable for SAV, thereby furthering SAV survival and persistence (Santos et al., 2012).

Cost-effective, large scale monitoring methods are fundamental to tracking and managing invasive aquatic plants. Remote sensing imagery (both aerial and satellite) is a non-intrusive and repeatable mapping method that has been widely used to map invasive aquatic plants (Ackleson and Klemas, 1987; Lehmann and Lachavanne, 1997; Sawaya et al., 2003; Ward et al., 2003; Zhang, 1998). Airborne hyperspectral imagery acquired at fine spatial resolution is more effective at discriminating aquatic species than the more widely available airborne and satellite multispectral imagery (Hestir et al., 2008; Santos et al., 2012; Silvestri et al., 2003). Hyperspectral imagery measures the solar spectrum from visible through the infrared and can contain hundreds of bands. Technically the difference between the hyperspectral imaging term and imaging spectrometry is that hyperspectral imaging simply implies lots of

spectral bands while imaging spectrometry indicates that you have many narrow spectral bands that cover a defined interval of the electromagnetic spectrum.

From 2004 to 2008, the Center for Spatial Technologies And Remote Sensing (CSTARS) conducted an extensive study using airborne hyperspectral imagery from the HyVista Corporation, the Australian HyMap instrument, to assess the extent of SAV and FAV species in the Delta, funded by the California Department of Boating and Waterways. Six years later, monitoring started again, this time funded through California Department of Fish and Wildlife (CDFW) drought funds and funds allocated for the Delta Smelt Resiliency Strategy (DSRS). Airborne AVIRIS-NG hyperspectral imagery was acquired over the entire Delta in fall of 2014 and 2015 and over the central Delta and Liberty Island in fall of 2016 and 2017. In 2018 and 2019, data was collected using the HyMap sensor again but at a finer resolution of 1.7 x 1.7 m. For the 2020 flight, SpecTIR delivered imagery at a resolution of 2x2 m pixels. The 2004, 2008, 2015, 2017, 2019 and 2020 results of classified SAV and FAV in the Delta are presented in this report highlighting trends and their possible causes.

3. Study Area Description

The Sacramento-San Joaquin River Delta spans approximately 2,219 km², extending from Sacramento, Yolo and Solano Counties in the north to the San Joaquin County in the south.

3.1 Habitat

The Delta is a diverse network of channels emptying the two major river systems of Northern and Central California into San Francisco Bay. While the Delta supports a great variety of habitats, characteristics of the two dominant physical habitats are described below:

3.1.1 Water Channels:

- a. Principal water channels are wide and deep and do not support macrophytic aquatic vegetation except along the shallow channel edges where water velocity is low,
- b. Channels with small natural islands support SAV and FAV in the shallow waters along the island's edge, and
- c. Narrow and shallow meandering sloughs in the east Delta that are frequently extensively colonized by either SAV or FAV.

3.1.2 Flooded Islands:

Arising from breached levees, they often have shallow water depths and support extensive patches of SAV and FAV. Emergent wetland species (EAV) like tules and cattails form a boundary at the leading edge of the land. Riparian vegetation on the levee crown protect the islands and act as a buffer to the strong winds, common in the Delta. These Deltaic lakes can be compared to shallow temperate lakes as open systems and low water velocity driven primarily by wind-wave action.

3.2 Aquatic Plant Communities

The aquatic vegetation in the Delta can be categorized into submerged, floating, and emergent plant communities, referred in this report as SAV, FAV and EAV (Table 3.1).

3.2.1 Submerged Aquatic Species (SAV):

The Delta SAV community consists of at least six native and four non-native species but is dominated by the invasive *Egeria densa* (Brazilian waterweed) (Hestir et al., 2008; Santos et al., 2010). The ecological niche of SAV species in the Delta, although limited by light availability and water velocity (Koch, 2001; Santos et al., 2010), is spatially much more extensive than that of the floating species.

3.2.2 Floating Aquatic Species (FAV):

The creeping emergent and floating macrophyte community in the Delta is dominated by two non-native species, water hyacinth (*P. crassipes*) and water primrose (*Ludwigia spp.*) (Cal-IPC, 2006; Khanna et al., 2011; Santos et al., 2009). There are also three native species, pennywort (*Hydrocotyle umbellata*), fairy moss (*Azolla spp.*) and duckweed (*Lemna spp.*). Both pennywort and water primrose, although nominally rooted, develop adventitious roots that can draw nutrients directly from the water, which allow them to form floating canopies extending several meters into the channel from the shore (Cook, 1990; Rejmánková, 1992). Hence, we consider them as part of the floating species class.

3.2.3 Emergent Aquatic Vegetation (EAV):

The emergent plant community in the Delta is dominated perennial monocots, including two *Typha* species (cattail), *T. latifolia* and *T. angustifolia* and their hybrids, two *Schoenoplectus* species (tule), *S. acutus* and *S. californicus*, and the invasive cane-like grass, *Phragmites australis* (common reed). In addition, there is another common invasive species, *Arundo donax* (giant cane), also a cane-like grass that is generally found on slightly higher ground on the levees adjoining the channels.

Table 3-1. Common names and scientific names of target species found in the Delta. Some species only have a few field points because they are relatively scarce in the Delta or not found in the parts of the delta where field data were collected. Number of times each species or type was identified in field-collected data points. A total of 838 points were measured.

Broad Class	Species (common name)	Species (scientific name)	2020 Points
Submerged Aquatic Vegetation (SAV)	Brazilian waterweed	<i>Egeria densa</i>	50
	Watermilfoil	<i>Myriophyllum spicatum</i>	18
	Coontail	<i>Ceratophyllum demersum</i>	12
	Fanwort	<i>Cabomba caroliniana</i>	5
	Curly leaf pondweed	<i>Pomatogeton crispus</i>	6
	American pondweed	<i>Potamogeton nodosus</i>	2
	Richardson's pondweed	<i>Potamogeton richardsonii</i>	5
	Sago pondweed	<i>Stuckenia pectinata</i>	10
	Waterweed	<i>Elodea canadensis</i>	3
	Southern Naiad	<i>Najas guadalupensis</i>	3
	Algae mats		3
	SAV mixed		62
Floating Aquatic Vegetation (FAV)	Water primrose	<i>Ludwigia</i> spp.	140
	Pennywort	<i>Hydrocotyle umbellata</i>	11
	Mosquito fern	<i>Azolla</i> spp.	7
	Water hyacinth	<i>Pontederia crassipes</i>	86
	Sponge plant	<i>Limnobium laevigatum</i>	1
Emergent Aquatic Vegetation (EAV)	Tule	<i>Schoenoplectus</i> spp.	122
	Common reed	<i>Phragmites australis</i>	37
	Giant reed	<i>Arundo donax</i>	15
	Cattail	<i>Typha</i> spp.	75
Water	Water		67
Other			98

4. Image Acquisition and Pre-processing

The Fenix 1K sensor was flown over the Delta between July 15-18 by SpecTIR LLC. as shown in Figure 4-1. Fenix measured 320 bands which collected data in wavelengths from 390 nm to 2450 nm (bandwidth: 5 nm). Flightlines were flown to overlap by 25% to avoid gaps in the data. The data was delivered at a resolution of 2x2m. The flightlines were geocorrected and atmospherically calibrated to reflectance by SpecTIR and delivered to CSTARS.

Figure 4-2 shows the location and pseudo true color views (that is, three bands in the blue, green and red parts of the visible spectrum that are displayed in true color) from seven sites that we chose to focus on during this study.

Table 4-1. Summary of image acquisition from 2004 to 2020.

Year	Image acquisition	# of Flightlines	Sensor	Pixel Size	Image area hectares	Image extent
2004	Jun 25 - Jul 7	64	HyMap	3.0m	274691.3	Full Delta
2005	Jun 22 - Jul 8	64	HyMap	3.0m	329149.7	Full Delta
2006	Jun 21 - 26	64	HyMap	3.0m	282437.8	Full Delta
2007	Jun 19 - 21	64	HyMap	3.0m	277178.2	Full Delta
2008	Jun 29 - Jul 07	48	HyMap	3.0m	219841.9	Liberty island to S. Delta
2014	Nov 14-25	61	AVIRIS	2.5m	239707.9	Full Delta
2015	Sep 17-21	61	AVIRIS	2.5m	317265.0	Full Delta
2016	Oct 8-9	22	AVIRIS	2.5m	104355.0	Liberty island, central Delta
2017	Nov 1	22	AVIRIS	2.5m	93874.2	Liberty island, central Delta
2018	Oct 6-9	42	HyMap	1.7m	184319.2	Liberty island to Lost slough, central Delta
2019	Sep 23-28	71	HyMap	1.7m	326098.9	Full Delta
2020	Jul 15-18	58	Fenix	2.0m	318763.3	Full Delta

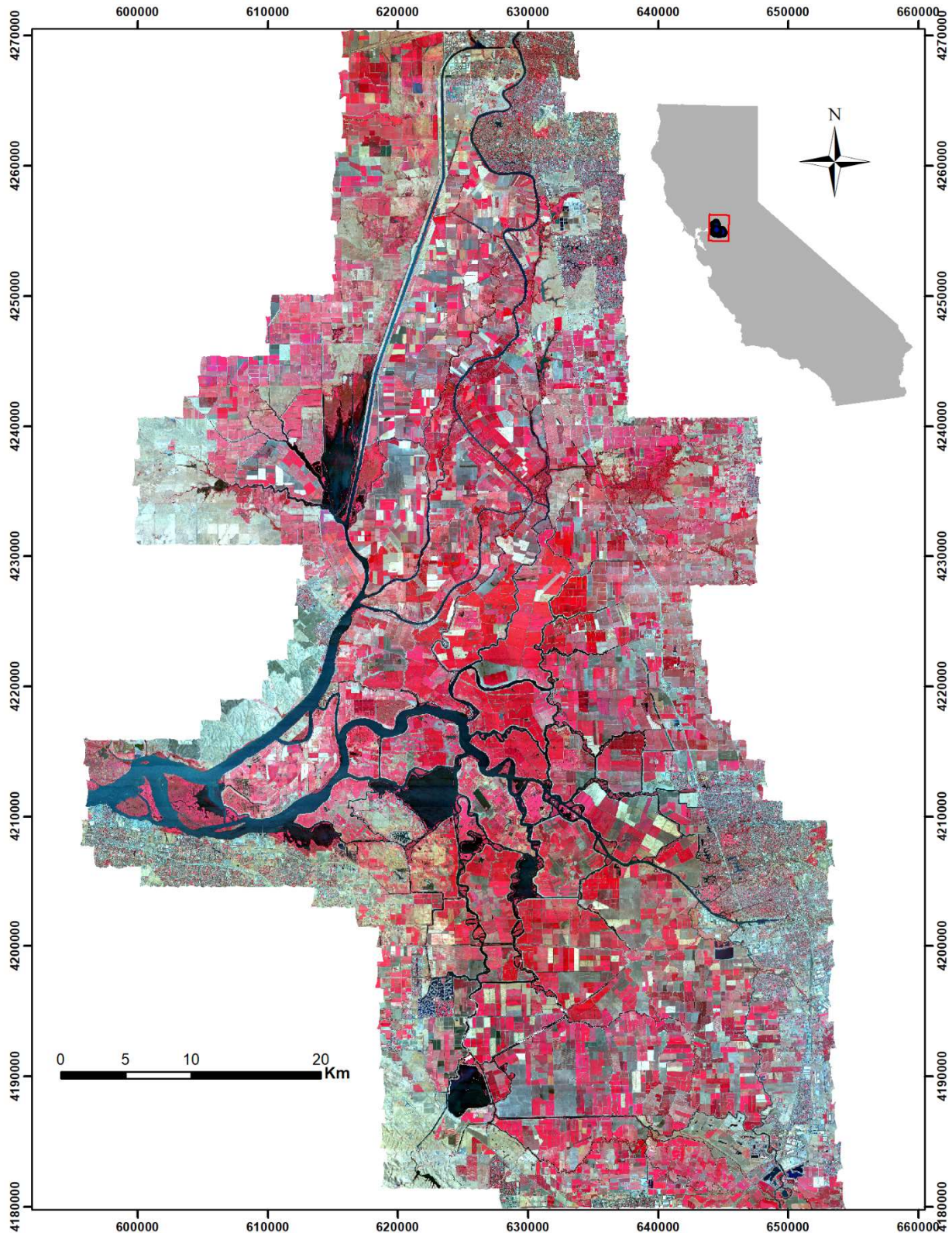


Figure 4-1. Color InfraRed band mosaic of the Delta imagery acquired in July 2020.

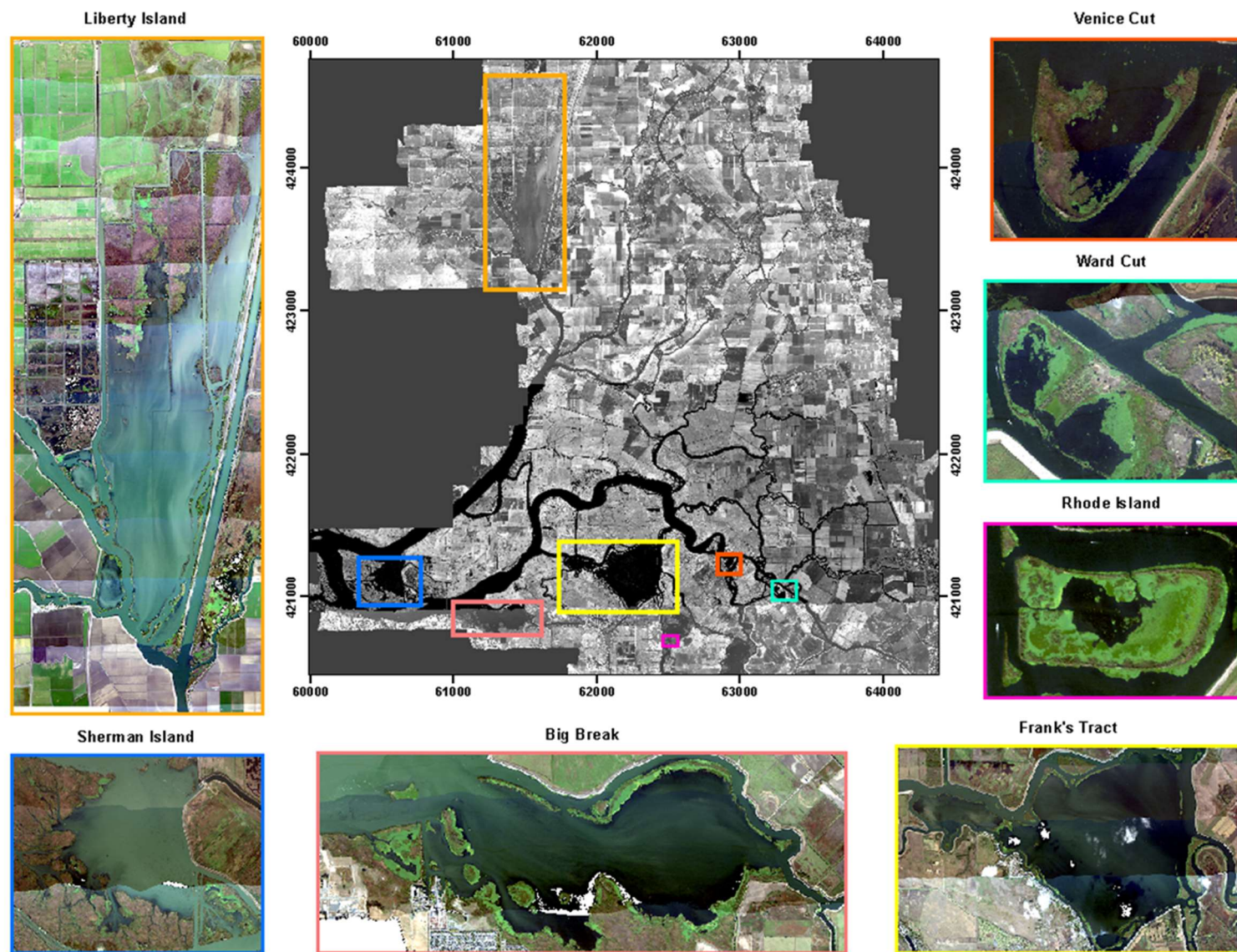


Figure 4-2. Location of study sites chosen to show detailed species maps.

5. Field Data Collection

Field work in support of the July 2020 overflights was done from July 20 - 31, 2020. Staff from CSTARS collected the data from motorboats provided by the California Department of Food and Agriculture. UC Merced also contributed personnel and boat for the Summer 2020 field campaign. These crews collected Ground Reference Data (GRD), noting the GPS location and species and other features (e.g., flower, vegetative, green or senescent) of aquatic vegetation species that were used in training and validation of the classified maps.

The crews collected 838 data points (Figure 5-1) for the dominant submerged (SAV), floating (FAV), and emergent (EAV) vegetation species in the Delta. For each point they noted attributes such as species name(s), location, cover estimates, patch size and orientation. In addition, for SAV species, teams also collected open water, rake data and Secchi depth. GRD points were collected in mostly homogeneous patches (greater than 80% of a single species or cover class) larger than 9 m² (3 m x 3 m).

Positions were measured using high precision (sub-meter accuracy) Trimble DGPS units (Trimble Navigation Limited, Sunnyvale, California) with Wide Area Augmentation System (WAAS) differential correction. If the observer was unable to center the DGPS on the weed patch, positions were recorded with a directional offset estimated using a combination of laser rangefinders, compass direction, and visual estimation. All GRD and DGPS positions were entered using a linked datalogger with TerraSync software (Trimble Navigation Limited) and exported as ArcGIS shapefiles projected to UTM Zone 10N, Datum WGS-84. Prior to training and testing of the classifier, the spatial and attribute data quality was checked through comparison of GRD, field photos, and imagery. Number of points collected for each species in 2020 are summarized in Table 3-1.

Table 5-1. Summary of ground reference data from 2004 to 2020.

Year	Image acquisition	Field GRD	Field Dates
2004	June 25 - July 7	2103	June 24 - July 2
2005	June 22 - July 8	2778	June 21-28
2006	June 21 - 26	4164	June 6-23
2007	June 19 - 21	2126	June 12-28
2008	June 29 - July 07	1334	June 23 - July 8
2014	November 14 - 25	1036	October 20-30
2015	September 17 -21	1375	September 9-17
2016	October 8-9	637	October 11-20
2017	November 1	891	October 3-11
2018	October 6-9	950	September 25 - October 3
2019	September 23 -28	1334	October 1-10
2020	July 15 -18	838	July 20-31, August 25

Table 5-2. Specific species of ground reference data collected from 2004 to 2020.

Common Name (scientific name)	2004	2005	2006	2007	2008	2014	2015	2016	2017	2018	2019	2020
Submerged Aquatic Vegetation (SAV) species												
Brazilian waterweed (<i>Egeria densa</i>)	432	601	1130	600	139	151	195	70	191	198	138	50
Watermilfoil (<i>Myriophyllum spicatum</i>)	69	36	68	184	30	43	33	21	30	44	28	18
American pondweed (<i>Potamogeton nodosus</i>)	25	30	63	42	7	3	7	0	7	3	2	2
Curly leaf pondweed (<i>Potamogeton crispus</i>)	25	19	44	117	22	20	40	25	26	20	7	6
Sago pondweed (<i>Stuckenia pectinata</i>)					21	48	48	15	7	27	5	10
Cabomba (<i>Cabomba caroliniana</i>)	12	7	15	34	8	21	2	8	18	9	17	5
Coontail (<i>Ceratophyllum demersum</i>)	29	15	17	221	68	31	45	6	4	23	23	12
Fine leaf pondweed (<i>Potamogeton filiformis</i>)						5						1
Common waterweed (<i>Elodea canadensis</i>)	5				1	22	4	1	2	4	7	3
Pondweed spp (<i>Potamogeton</i> spp.)	23	14	24	88								
Richardson pondweed (<i>Potamogeton richardsonii</i>)										8	14	5
Southern Naiad (<i>Najas guadalupensis</i>)										3	1	3
Algae	81	47	79	392	33	8	11	8	0	18	13	3
Mixed SAV	39		5	71	5	32		46	16	4	9	62
Other SAV	26	1	22									
Floating Aquatic Vegetation (FAV) species												
Water hyacinth (<i>Pontederia crassipes</i>)	262	304	285	58	93	223	284	104	116	128	115	86
Pennywort (<i>Hydrocotyle umbellata</i>)	201	300	400	313	87	13	11	4	15	12	2	11
Water primrose (<i>Ludwigia</i> spp.)	71	86	130	186	34	91	172	174	207	172	281	140
Mosquito fern (<i>Azolla</i> spp.)	12	5	7	1	2	5	2	2	9	13	19	7
Duckweed (<i>Lemna</i> spp.)		6		9		4	5	0	0	9		
Sponge plant (<i>Limnobium laevigatum</i>)										4		1
Parrot feather (<i>Myriophyllum aquaticum</i>)			3		1							
Emergent Aquatic Vegetation (EAV) & Riparian												
Cattail (<i>Typha</i> spp.)	54	31	14	50	6	56	52	38	53	37	81	75
Tule (<i>Schoenoplectus</i> spp.)	259	363	291	376	47	173	98	69	64	72	219	122
Common reed (<i>Phragmites australis</i>)	26	42	31	39	0	22	44	12	6	17	24	37
Giant reed (<i>Arundo donax</i>)	33	55	102	16		32	54	8	21	24	25	15
Riparian	174	250	905	84	4							
Water	86	53	352	912	720		239	5	47	73	122	67

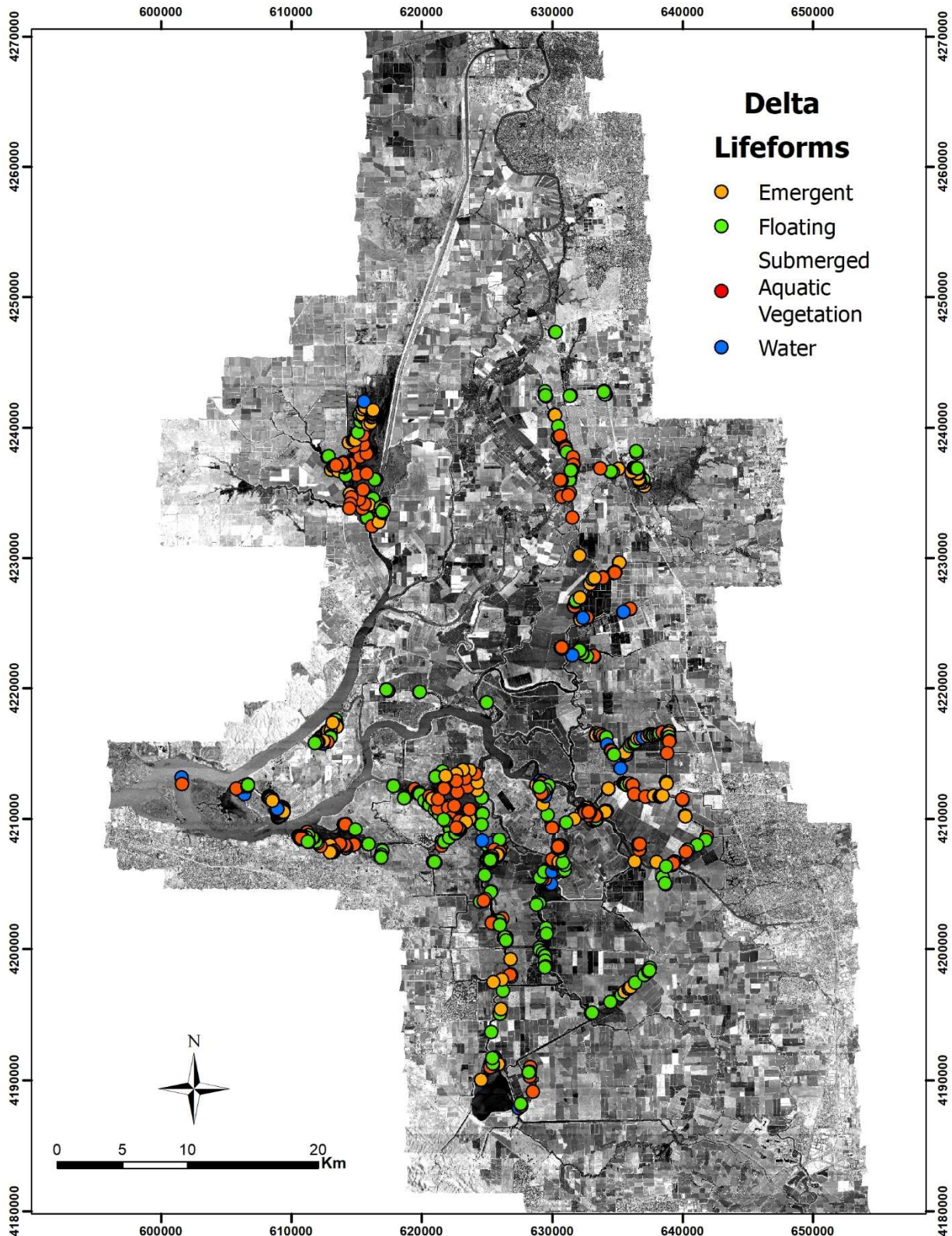


Figure 5-1. Location of field data collected in July 2020. The lifeform points are enlarged to show up clearly.

6. Image Classification

6.1 Data Reduction Techniques

Three different data reduction techniques (or data enhancement techniques) were used to create the inputs fed into the Random Forests classifier. While Spectral Mixture Analysis (SMA) and Spectral Angle Mapper (SAM) are themselves classifiers, in this analysis, they were used to highlight the most important spectral differences between the species and cover types and not as independent classifiers.

6.1.1 Indexes

Indexes are single values generated by combining data from multiple spectral bands. Indexes highlight and enhance certain spectral properties while reducing background effects that would normally depress the spectral identification. For each flightline, we calculated a suite of parameters that included various indexes sensitive to differences in plant biochemistry, such as NDVI (sensitive to leaf mass or area), NDWI (sensitive to leaf water content), and GI (sensitive to differences in chlorophyll concentration). Indexes allow us to approach the underlying biophysical parameters of different land cover classes, however they are empirical relationships and may respond differently to different plant communities or under different environmental conditions. All calculated indexes are described in Table 6-1 along with their formulas and relevant scientific sources.

6.1.2 Spectral Mixture Analysis (SMA)

Spectral mixture analysis (SMA) was used to calculate the within-pixel fractional cover of the general landcover classes. In SMA, the model estimated fractions of the endmembers are adjusted using the least squares method until the best spectral fit is found to match the band-by-band measured pixel spectrum, plus any residual error (Adams et al., 1995; Huete, 1986; Smith et al., 1990). The method can theoretically identify as many endmembers (the reference spectra) as is equal to the number of bands plus one additional band for Root Mean Square Error (RMSE). However, if you use more than a few endmembers for calculating the endmembers in a pixel, you run into the problem that some endmembers can be created by combining the spectra of other endmembers, thus only the most distinctive endmembers are used. We selected six general types of endmembers for the SMA: water, soil, dry plant residues (Non-Photosynthetic Vegetation: NPV), SAV, FAV and EAV. For each image pixel, the fractional cover of each SMA endmember is calculated as the proportion of the measured spectrum for that pixel. Figure 6-1 A shows the spectral library used for the SMA.

6.1.3 Spectral Angle Mapper (SAM)

Spectral Angle Mapper (SAM) uses the full spectrum, which is calculated as a vector, to define each reference class. This method uses an n -Dimensional angle to confirm the match of unknown pixel spectrum to a reference spectrum. The algorithm determines the similarity between the two spectra by calculating the angle between them, treating them as vectors in space with dimensionality equal to the number of bands. This technique is relatively insensitive to illumination and albedo effects, common artifacts in image data. Smaller angles represent closer matches to the reference spectrum and greater likelihood that the unknown pixel is of the same class as the reference spectrum. For the class image, each pixel is assigned to the class that forms the smallest angle (Kruse et al., 1993).

Analyses for multiple reference spectra are run sequentially on the images, each one producing a map for the probable distribution of that reference class. The analyst must then decide where to assign boundaries for overlapping classes. SAM has been shown to be highly effective for identifying aquatic vegetation (Alberotanza, 1999; Hirano et al., 2003; Merenyi et al., 2000). Spectral libraries with SAM files were created separately for SAV, FAV and EAV communities and for clear and turbid water (Figure 6-1 B). SAM produces rule images that contain as many bands as there are endmembers. Each band is the estimated distance of the pixel spectrum from the reference spectrum corresponding to that band. Only the rule images were used in our analysis, ignoring the classification images produced by SAM.

6.1.4 Continuum Removal

Many hyperspectral mapping and classification methods require the data to be calibrated to percent reflectance. Continuum removal is a method that helps to identify the presence of absorption features and provides a basis for comparison of absorption depth, shape, and symmetry. It fits a generalized spectrum without specific absorption features to the measured spectrum with such features. The difference in reflectance between the two spectra is the measured variable. The continuum is a mathematical function that is used to isolate absorption features for analysis (Clark and Roush, 1984). It is the equivalent of a “background signal” of the material if specific absorption features of interest were not present. Spectra are normalized to a common reference using a continuum formed by defining shoulders at the edges of the absorption features. These are “high points” in the spectrum (local maxima) and straight lines are fit across the spectral segments between these points. The continuum is “removed” by dividing the original spectrum by the continuum. In this way, the spectrum is normalized for albedo and the relative strengths of the absorption features can be quantified. In this study, we applied three continuum removals between the spectral ranges of 907-1047, 1073-1293, and 2209-2384 nm.

Table 6-1. Indexes used as inputs to the Random Forests classifier.

No.	Acronym	Formula	References
1	NDVI	$(R_{NIR} - R_R)/(R_{NIR} + R_R)$	(Tucker, 1979)
2	gNDVI	$(R_{750} - R_G)/(R_{750} + R_G)$	(Gitelson et al., 1996)
3	mNDVI	$(R_{750} - R_{700})/(R_{750} + R_{700})$	(Gitelson and Merzlyak, 1994)
4	RG_Ratio	R_R/R_G	(Gamon and Surfus, 1999)
5	NDII	$(R_{NIR} - R_{923})/(R_{NIR} + R_{923})$	Adapted from (Hunt and Rock, 1989)
6	NDII2	$(R_{NIR} - R_{SWIR})/(R_{NIR} + R_{SWIR})$	(Hunt and Rock, 1989)
7	LPI	$1/R_G - 1/R_{NIR}$	adapted from (Gitelson et al., 2002)
8	ANIR	angle: $R_R, R_{NIR} \& R_{SWIR}$	(Khanna et al., 2007)
9	ARed	angle: $R_G, R_R, \& R_{NIR}$	(Khanna et al., 2013)
6	ASWIR1	angle: R_R, R_{NIR}, R_{SWIR}	(Khanna et al., 2007)
11	GI	$(R_G - R_R)/(R_G + R_R)$	(Motohka et al., 2010)
12	PRI	$(R_{530} - R_{570})/(R_{530} + R_{570})$	(Gamon et al., 1990)
13	CAI	$0.5*(R_{2020} + R_{2220}) - R_{2100}$	(Nagler et al., 2000)
14	WADI	$(R_{1070} - R_{1167})/(R_{1070} + R_{1167})$	Water Absorption Difference Index
15	ADW1	$0.5*(R_{1070} + R_{890}) - R_{990}$	(Khanna et al., 2013)
16	ADW2	$0.5*(R_{1270} + R_{1070}) - R_{1167}$	(Khanna et al., 2013)
17	SIFI	$(R_{800} - R_{445})/(R_{800} - R_{680})$	(Peñuelas et al., 1995)
18	CRI_550	$1/R_{510} - 1/R_{550}$	(Gitelson et al., 2002)
19	CRI_700	$1/R_{510} - 1/R_{700}$	(Gitelson et al., 2002)
20	ARI	$1/R_{550} - 1/R_{700}$	(Gitelson et al., 2001)

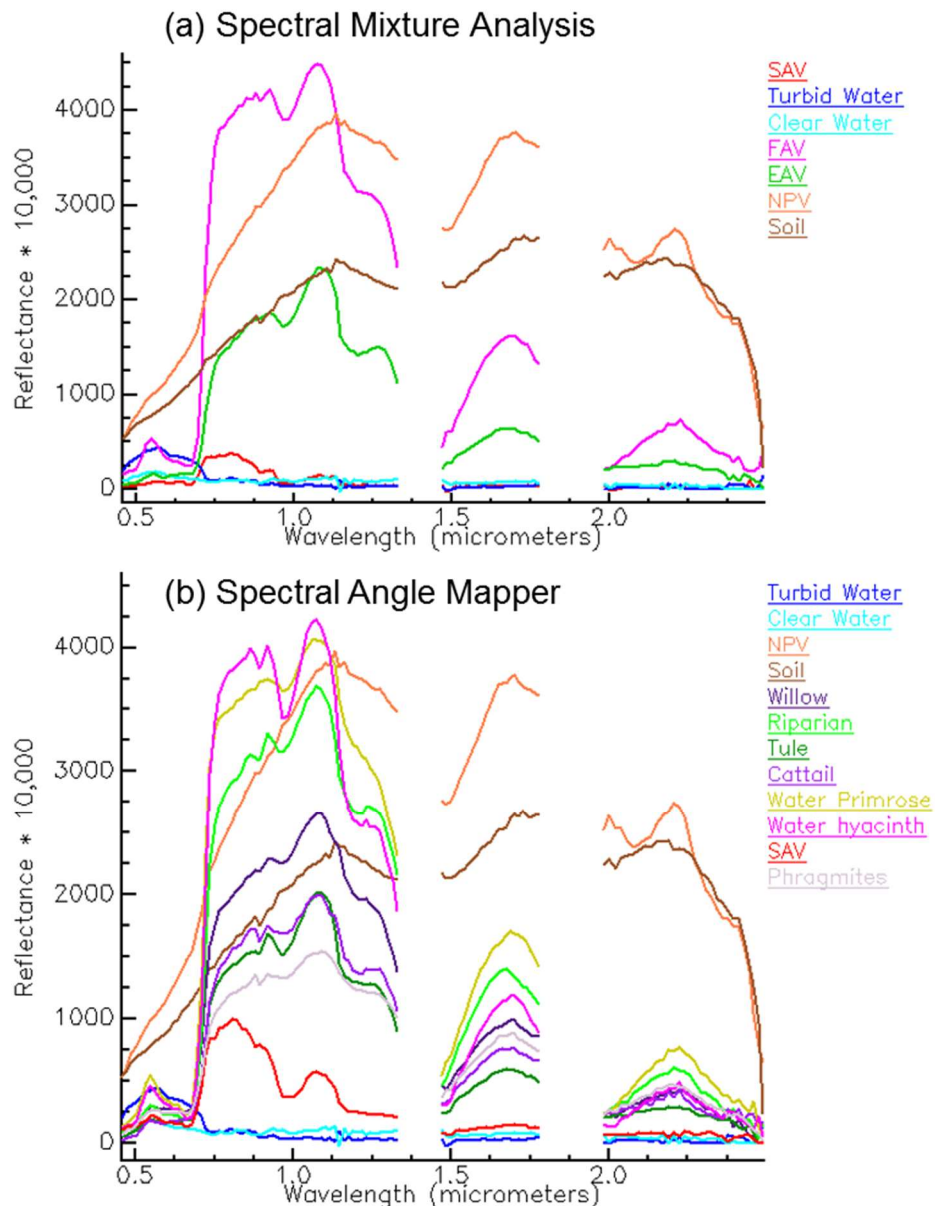


Figure 6-1. Spectral libraries used to run the (A) Spectral Mixture Analysis (SMA) and the (B) Spectral Angle Mapper (SAM)

A total of 55 different parameters (indexes, bands, SMA and SAM) were created using the 320 bands of imagery. Entire list of inputs used, along with their acronyms and full names are tabulated in Appendix A. These are the inputs used to train the classifier.

6.2 Classifier

The inputs from the above three procedures were combined in a single file for each flightline. Training data was extracted from the consolidated files and used to train the classifier. During the analysis of the 2014 data, we tested three non-parametric classifiers, all of which are insensitive to the type of inputs, spread of the data, etc. Our tests showed that Random Forests performed the best of the three

classifiers hence in succeeding years we have only classified images using the Random Forests approach. A brief explanation of the Random Forests classifier is provided below.

Random Forests is an automated algorithm that builds hundreds of tree models (Breiman, 2001) by randomly selecting a subset of the training data to classify each tree. This is repeated many times to develop a large set of trees that are used to determine the best fit class type for each pixel. To classify a new object from an input vector, it passes the input vector down each of the (classification) trees in the "forest" (the set of trees). Each tree provides a classification termed a "vote" for a class. The type of forest is chosen by the classification type having the most "votes" (i.e., the most frequently chosen class among all the trees identified for each pixel). Each tree is grown to the largest extent possible. There is no pruning. But because the classifier produces a forest of trees and then "chooses" the most frequently selected class, it limits the problem of over-fitting, which occurs when an algorithm becomes too specific to the training data thus losing accuracy when trying to classify test data.

7. Results

7.1 Accuracy Assessment

The field data was split equally into training and test datasets. Polygons were created after considering the field data point description and looking at the corresponding field photos. Points are not always taken in the center of a patch and sometimes are taken alongside a patch, sometimes using a rangefinder offset. Hence the field data point did not always lie in the center of the created polygon. The polygon size varied with the patch size information that was collected in the field. Training polygons were only used for training the classifier and test data were only used for accuracy assessment maintaining the separation between test and training data. A confusion matrix was used to calculate the overall accuracy, user's and producer's accuracies, and the Kappa statistic (Story and Congalton, 1986). The overall accuracy indicates the probability that the species identified in the image map is in agreement with field data at the location. The user's accuracy indicates the probability that an image pixel labeled as a certain class is really that class at the field location; this type of test calculates what is often called commission error. The producer's accuracy indicates the probability that the species identified at a field location is correctly mapped in the image, which is an estimate of the omission error. The Kappa statistic indicates the level of overall agreement between the field data and the classification map. It takes into account the probability of random agreement between the field data and classification results (Lillesand et al., 2004; Rosenfield and Fitzpatrick-Lins, 1986). Kappa values range from 0 to 1 with values greater than 0.5 indicating good agreement and values greater than 0.8 indicating exceptional agreement between the two data sets.

Table 7-1: Confusion matrix for Random Forests Classifier for the year 2020. EMPR: emergent marsh invaded by water primrose; SAV: submerged aquatic vegetation; NPV: non-photosynthetic or dry vegetation.

Classified as	Reference Field Data Points												Total	User's Accuracy
	Arundo	EMPR	NPV	Phragmites	Riparian	SAV	Shadow	Soil	Tule-Cattail	Water	Water hyacinth	Water primrose		
Arundo	250	0	0	6	1	0	0	0	0	0	0	6	263	95.1
EMPR	21	1579	0	4	4	0	0	0	39	0	131	72	1850	85.4
NPV	0	0	2272	0	0	0	0	16	2	0	14	0	2304	98.6
Phragmites	0	0	0	155	20	0	0	0	28	0	2	0	205	75.6
Riparian	40	81	2	45	1652	0	0	0	114	0	23	18	1975	83.6
SAV	0	0	3	0	0	2222	45	0	32	26	8	0	2336	97.0
Shadow	0	0	0	0	0	54	981	0	1	4	0	0	1040	99.5
Soil	0	0	212	0	0	3	0	2479	0	0	0	2	2696	92.0
Tule-Cattail	10	41	4	44	86	26	0	5	1440	0	104	18	1778	81.0
Water	0	0	0	0	0	188	65	0	0	2464	0	0	2717	90.7
Water hyacinth	2	96	6	1	10	2	0	0	28	0	2118	30	2293	92.4
Water primrose	46	6	0	0	15	0	0	0	14	0	100	1531	1712	89.4
Total	369	1803	2499	255	1788	2495	1091	2500	1698	2494	2500	1677	21169	
Producer's Accuracy	67.8	87.6	90.9	60.8	92.4	91.2	94.0	99.2	84.8	98.8	84.7	91.3		90.4

Table 7-1 shows the confusion matrix for the Random Forests (RF) classifier for the Summer 2020 as calculated for the Delta region. The overall accuracy was 90.4% while the Kappa was 0.89. Accuracy for previous years is also shown in Table 7-2.

Table 7-2: Overall accuracy and Kappa Coefficients for all years of datasets cited in this report.

Year	Overall Accuracy	Kappa Coefficient	N
Summer 2004	88.8	87.0	8247
Summer 2005	91.5	90.5	36593
Summer 2006	88.4	87.1	15788
Summer 2007	89.2	87.7	7572
Summer 2008	88.9	87.2	6704
Fall 2014	81.8	78.9	13906
Fall 2015	91.8	90.1	15284
Fall 2016	87.4	85.3	11989
Fall 2017	85.5	76.1	14583
Fall 2018	90.2	89.0	20874
Fall 2019	90.5	89.6	31944
Summer 2020	90.4	89.4	21169

Every single year was reclassified to ensure that the shadow class and riparian class were mapped in addition to other classes. The final target classes mapped consistently for all years since 2004 were: water, SAV, soil, non-photosynthetic vegetation, emergent marsh, riparian vegetation, and shadow. The color scheme was also standardized for all years. Generally, the spectrum of a tree shadow falling over water is very similar to a SAV pixel spectrum. Remote Sensing optical imagery has the disadvantage that

spectrum is mainly a reflection of the top layer of landcover within the pixel. This means that when riparian trees overshadow the waterways, the sensor is mainly “seeing” the tree, not the vegetation that might be under the tree. Hence, it is important to map shadow as shadow because we don’t really know if the sensor is receiving much information from the vegetation in the water column underlying the tree shadow.

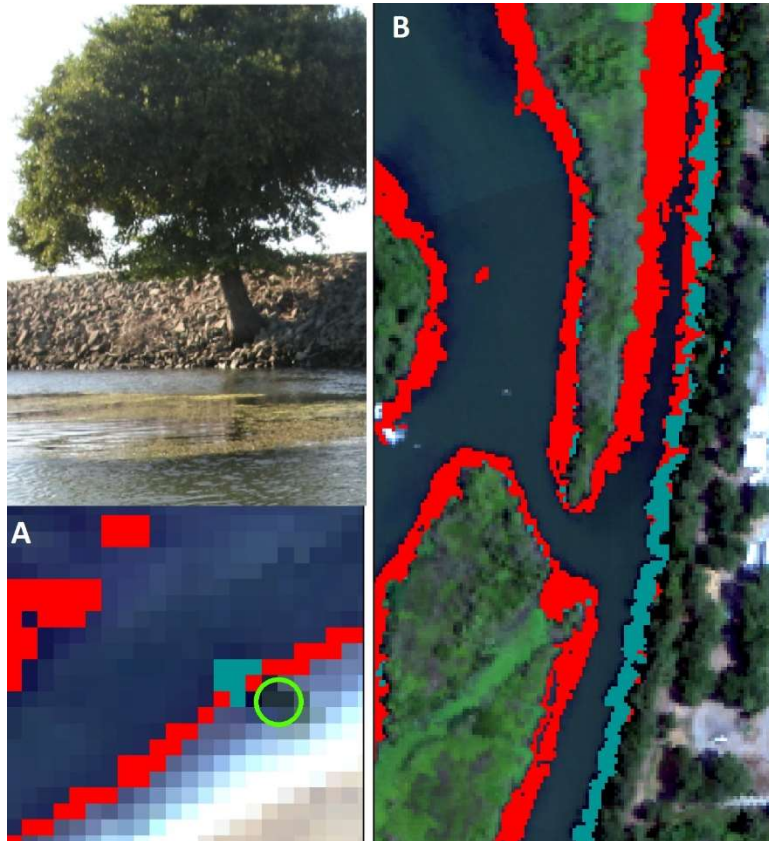


Figure 7-1: Performance of the shadow classification. Red represents SAV and dark cyan represents shadow class. The upper left panel shows a tree in a channel that has SAV growth along the channel edge. (A) shows the class image with SAV along the edge but the pixels under the tree classified as shadow. (B) shows shadow mapped along the channel edge on the shadow side.

The shadow class was largely successful in preventing false positives for SAV detection (Figure 7-1) although some SAV might still be mapped as shadow. Overall, this misclassification was rare and within the uncertainty estimates of our classifier.

Another problem we faced in 2019 and 2020 which had been rare in previous years, was the abundance of mixed pixels of emergent marsh and water primrose. Due to the recent incursions of water primrose into emergent marsh, when water primrose mats were interwoven within the marsh, the mixed class, in terms of its spectra, behaved neither like pure water primrose nor like marsh but instead was closer to the riparian tree signature. Figure 7-2 A shows how the transition between primrose mats and marsh were mapped as riparian vegetation in 2019 and Figure 7-2 C shows what the area looks like in the true color image. In 2020, we decided to map a new class called EMPR (emergent marsh invaded by water primrose). Figure 7-2 B shows the same region in Liberty Island with this special mixed class mapped

separately. The right and lower panels show field pictures of invaded marsh. Mapping the mixed class as a separate class likely increases uncertainty of water primrose, marsh and the mixed class maps, but it is preferable over calling this class either primrose or emergent marsh. Our accuracy estimates for mapping this class are quite good with both user's and producer's accuracy being over 85%.

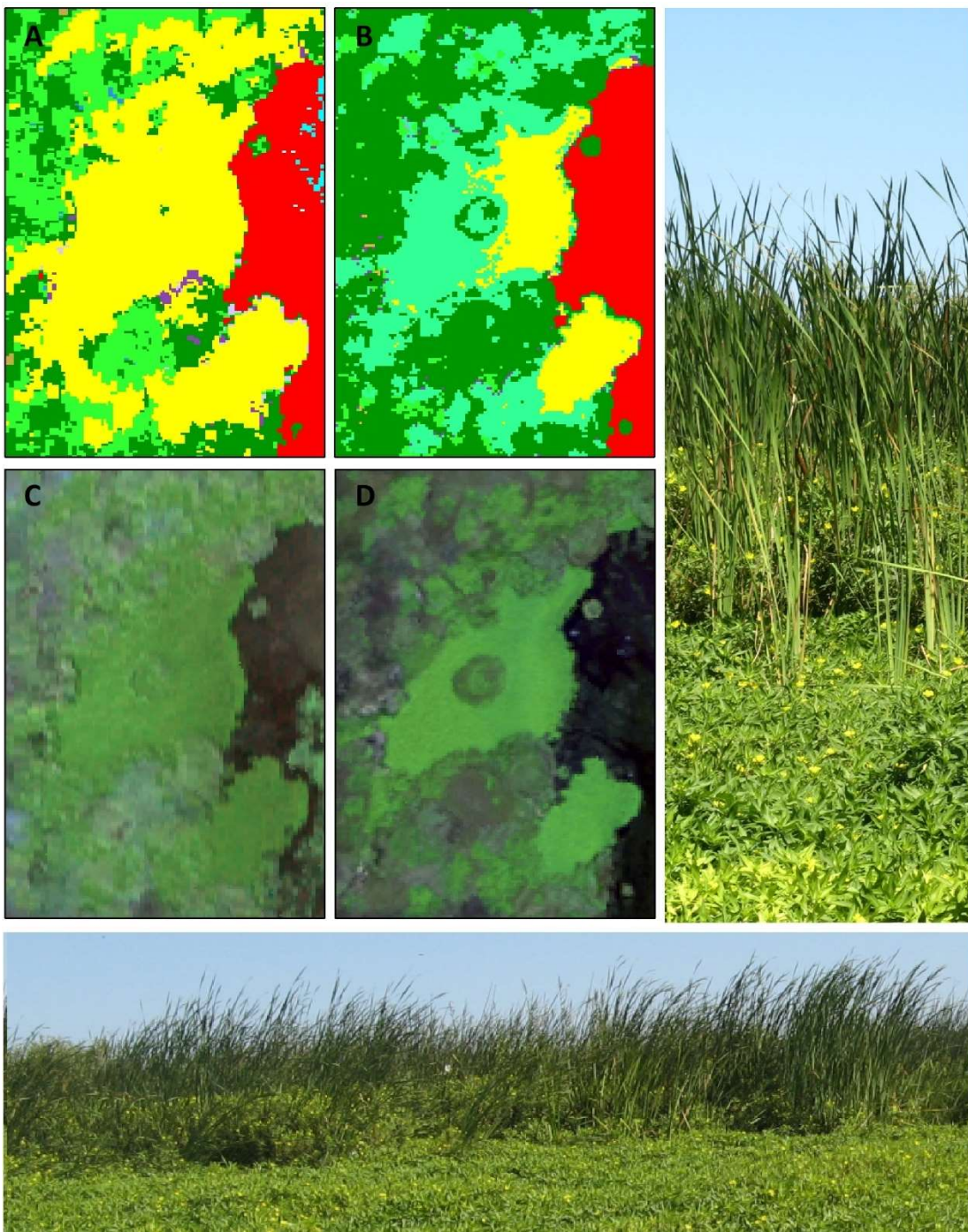


Figure 7-2: Water primrose invaded marsh field pictures (right panel and bottom panel) with (A) 2019 classification of water primrose (yellow) and the invaded marsh mapped as riparian (light green), (B) 2020 classification of invaded marsh as a separate class (chartreuse), (C) and (D) the 2019 and 2020 invaded marsh in true color.

7.2 Acreage Calculations

Total acreage values of submerged (SAV) and floating (FAV) species in hectares from the common area for all years in the Delta are listed in Table 7-3 (also see Figure 7-3) for 2004 to 2020 but the values represent area only in the region of the Delta common to all years – the Central Delta and the Liberty Island – Cache Slough complex.

Table 7-3: Area in hectares of Submerged Aquatic Vegetation (SAV), shadow, water hyacinth, water primrose, total Floating Aquatic Vegetation (FAV), within the common area (Central Delta + Liberty Island Cache Slough complex).

Year	Area (ha) for common area among all years					
	SAV	Shadow	Water hyacinth	Water primrose	Pennywort	Total FAV
Summer 2004	2558	161	234	280	129	643
Summer 2005	2284	175	153	125	98	375
Summer 2006	2457	377	369	171	102	641
Summer 2007	2442	338	74	183	107	364
Summer 2008	1161	549	83	157	142	382
Fall 2014	2094	1050	806	272	0	1,078
Fall 2015	3436	835	299	390	22	711
Fall 2016	2881	1379	185	456	0	641
Fall 2017	4293	621	108	671	0	779
Fall 2018	4416	689	181	473	0	654
Fall 2019	3987	377	195	599	0	794
Summer 2020	3776	158	232	514	0	746

Table 7-4: Percent cover of waterways for Submerged Aquatic Vegetation (SAV), shadow, water hyacinth, water primrose, total Floating Aquatic Vegetation (FAV), within the common area (Central Delta + Liberty Island Cache Slough complex).

Year	% of waterways for common area among all years					
	SAV	Shadow	Water hyacinth	Water primrose	Pennywort	Total FAV
Summer 2004	15.7%	1.0%	1.4%	1.7%	0.8%	3.9%
Summer 2005	14.0%	1.1%	0.9%	0.8%	0.6%	2.3%
Summer 2006	15.1%	2.3%	2.3%	1.1%	0.6%	3.9%
Summer 2007	15.0%	2.1%	0.5%	1.1%	0.7%	2.2%
Summer 2008	7.1%	3.4%	0.5%	1.0%	0.9%	2.3%
Fall 2014	12.9%	6.4%	4.9%	1.7%	0.0%	6.6%
Fall 2015	21.1%	5.1%	1.8%	2.4%	0.1%	4.4%
Fall 2016	17.7%	8.5%	1.1%	2.8%	0.0%	3.9%
Fall 2017	26.4%	3.8%	0.7%	4.1%	0.0%	4.8%
Fall 2018	27.1%	4.2%	1.1%	2.9%	0.0%	4.0%
Fall 2019	24.5%	2.3%	1.2%	3.7%	0.0%	4.9%
Summer 2020	23.2%	1.0%	1.4%	4.8%	0.0%	6.2%

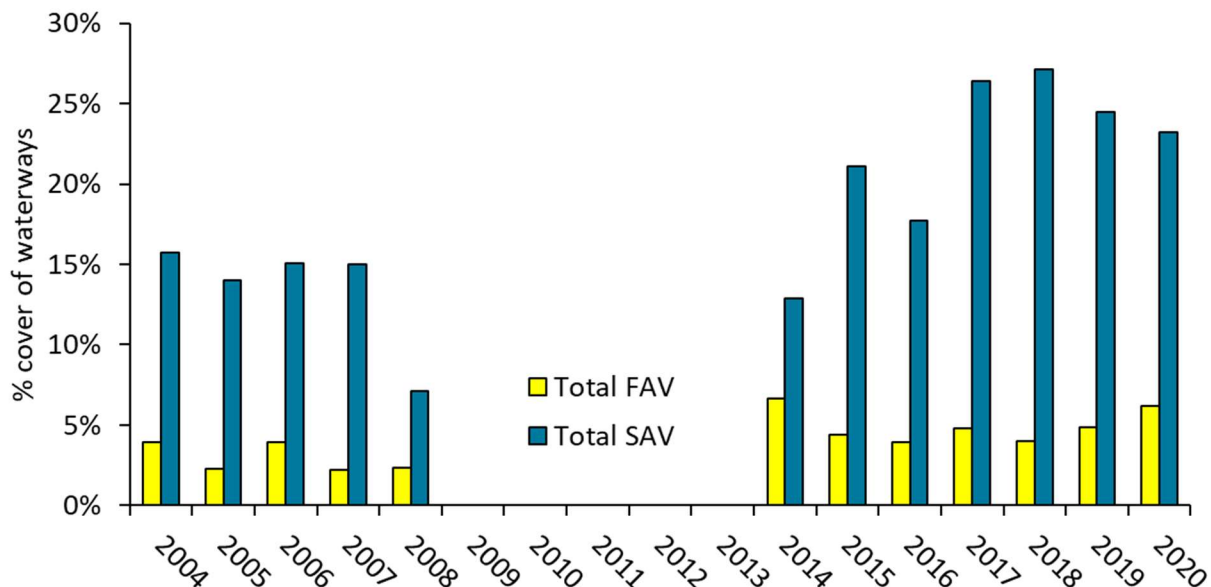


Figure 7-3: SAV as % cover of waterways for all available years (2009-2013 data gap)

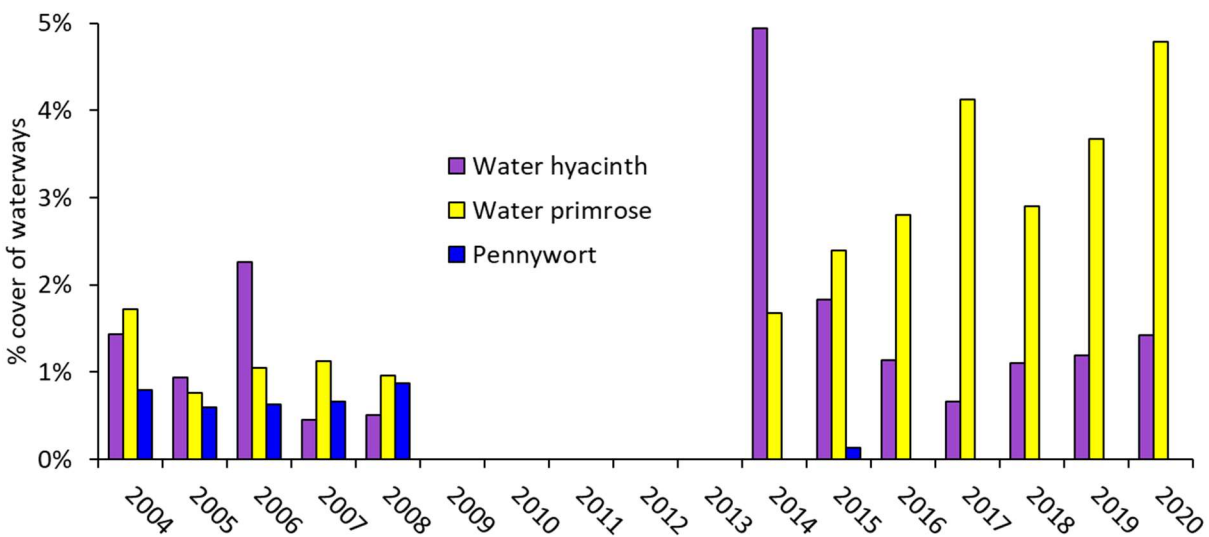


Figure 7-4: FAV total and by species as % cover of waterways for all available years (2009-2013 data gap)

The legal Delta imagery was acquired in 2004-2007, 2014, 2015, 2019, and 2020. All other years, the area acquired did not cover the entire Delta. Hence, figures 7-5 and 7-6 show the FAV and SAV cover for only those years when the entire extent was acquired.

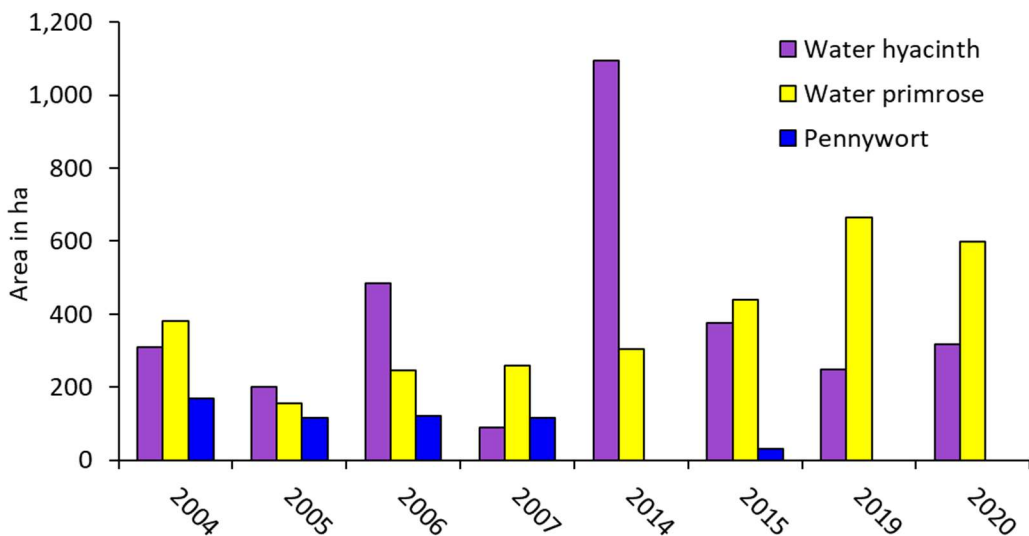


Figure 7-5: FAV species cover in hectares for all years that the Legal Delta imagery was captured.

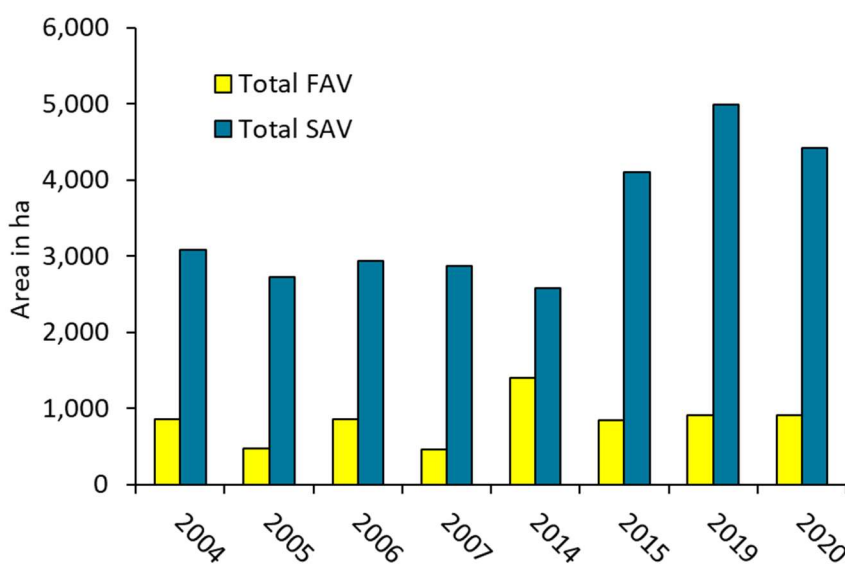


Figure 7-6: Total FAV and SAV cover in hectares for all years that the Legal Delta imagery was captured.

The total area in hectares for the Legal Delta are catalogued in Table 7-5. The maximum area of SAV recorded in the Delta is almost 5000 hectares and for FAV is almost 1400 hectares. The hectares recorded here *do not include* the SAV and FAV cover within restoration sites that have become tidally active in recent years (post-2014) in order to provide a fair comparison with previous years (2004-2008) when these sites were leveed off and not connected to the aquatic Delta. However, we did map the restoration sites and have noted that these invasive species have infiltrated many of the sites making it difficult to achieve management objectives for those sites.

Table 7-5: FAV species and total cover and SAV cover in hectares for all years that the Legal Delta was captured.

Year	% of waterways for common area among all years					
	SAV	Shadow	Water hyacinth	Water primrose	Pennywort	Total FAV
Summer 2004	3084.8	194.4	308.9	381.6	169.2	859.6
Summer 2005	2725.4	232.1	201.1	156.2	116.2	473.6
Summer 2006	2933.3	470.4	484.7	246.6	122.7	854.1
Summer 2007	2865.0	498.5	90.9	260.2	116.6	467.7
Fall 2014	2574.5	1941.7	1094.0	303.6	0.0	1397.6
Fall 2015	4107.7	951.0	376.8	439.8	30.2	846.7
Fall 2019	4988.6	485.9	247.5	663.9	0.0	911.4
Summer 2020	4421.9	182.8	318.7	598.5	0.0	917.2

With this long dataset dating back to 2004, we have observed many changes within the Delta. The total extent of invaded waterways has increased from the early period (less than 10% of waterways in 2008) to current (31% of waterways in 2017 and 2018). SAV also seems to have increased during the recent drought and now occupies ~10% more of waterways than it did in the early period (2004-2008; ~15%). This change has come gradually with the invasion of new habitat that used to be SAV-free in early years, for example, Liberty Island (see Figure 8-5).

The floating vegetation community has also changed in significant ways. While water hyacinth cover doesn't show a trend over time, in 2014, it was the highest ever when the Division of Boating and Waterways control program for water hyacinth got delayed. 2014, being a peak drought period, recorded the highest ever cover of total FAV (1400 hectares), dominated by water hyacinth. In the early period, FAV was co-dominated by three genera, the native pennywort, and the invasive water hyacinth and water primrose. But in recent years, pennywort has been outcompeted by the invasives (Figures 7-3 to 7-6) only showing up in spring and disappearing by summer (personal observation). Hence, it has been hard to find enough pennywort patches to train the classifier for the summer and fall imagery.

Water primrose has been the greatest species of concern among floating aquatic invasives due to its ability of invading marsh and replacing it (Khanna et al., 2018b). This species has expanded its cover in the Delta in the past two decades (Figure 7-4). It has also spread into areas slated for restoration like Prospect Island, making it difficult to engineer healthy restored ecosystems. In recent years, we have observed an acceleration of the invasion of water primrose into remnant Delta marshes. A study geared towards understanding the mechanisms that make this species a great invader and allow it to replace marsh has been funded under Prop 1. The same study will also quantify the movement of the invasion front of water primrose into vulnerable marshes.

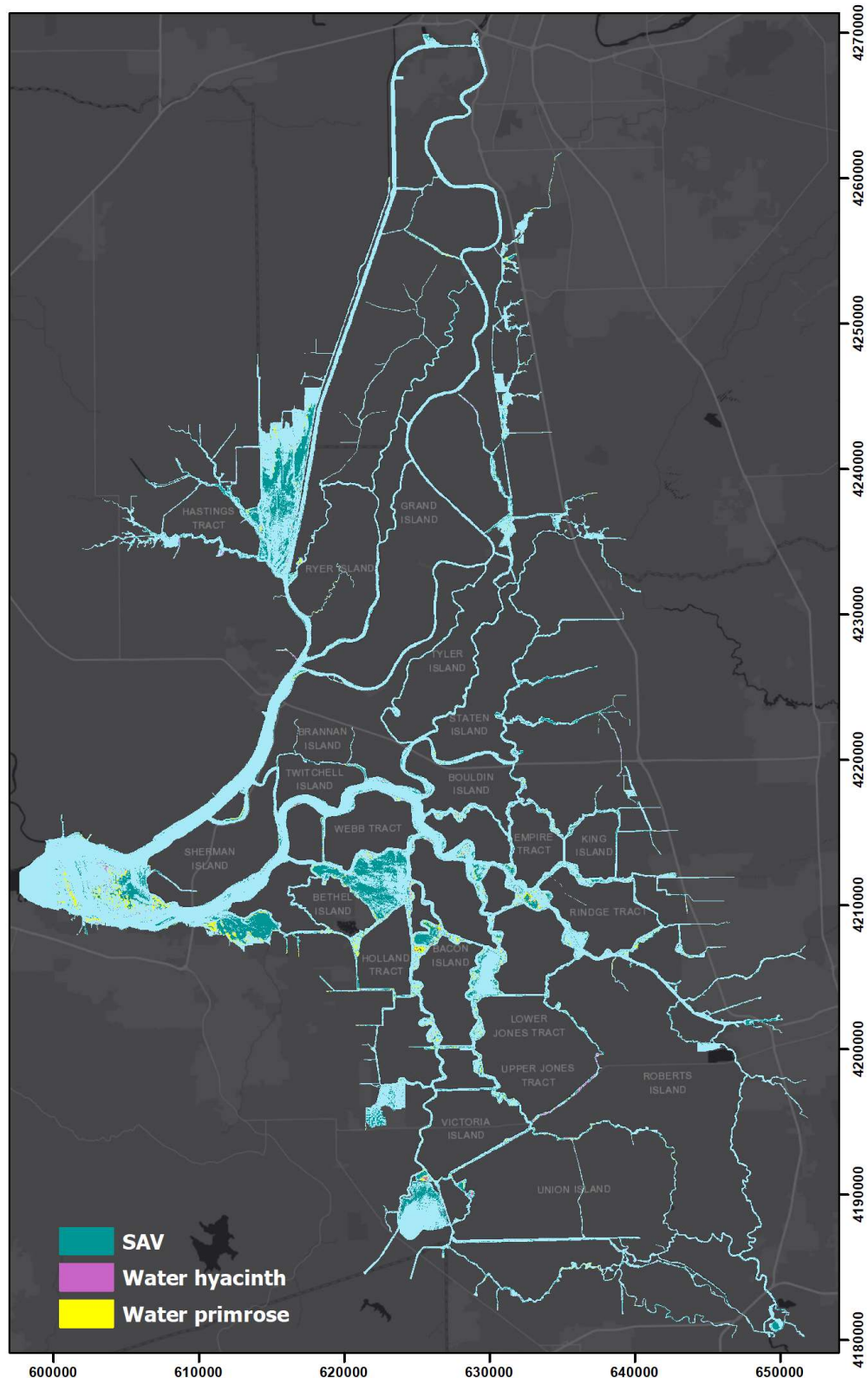


Figure 7-7. Submerged aquatic vegetation (SAV), water hyacinth and water primrose classification across the Central Delta and Liberty Island in July 2020.

8. Key Questions to be Addressed

8.1 Ideal Window for Image Acquisition

The IEP Report on monitoring of aquatic species recommended two acquisitions per year, one in spring, and one in fall to get a pre-treatment condition estimate and a post-treatment condition estimate of invasive species cover (Khanna et al., 2018a). On completing analysis of 2004-2008 and 2020 summer imagery, 2014-2019 fall imagery and the 2019 spring imagery, we recommend that the ideal timing for collecting imagery with the *aim of mapping the maximum extent of invasive species is in August* of every year. Our reasoning behind this recommendation is described below:

Without the intervention of a treatment program, the extent of invasive species cover would potentially reach its peak in October, right before the vegetation starts to senesce in November. However, DBW starts treating SAV and FAV in March and continues until October tapering off in November (DBW, 2018). Thus, there is new growth due to the summer growing season while there is die-off due to treatment. Hence, capturing imagery in October does not necessarily lead to mapping the maximum extent of cover. Furthermore, by October, the sun is lower in the sky leading to greater flightline edge effects. Higher winds in fall also lead to speckle on the larger open water areas. Both these factors increase errors in aquatic vegetation mapping.

In spring, sun angle is still low leading to higher flightline edge effects. Moreover, the vegetation is just beginning to grow hence it is harder to find training and validation data in the field for species of interest such as water hyacinth, water primrose, etc. These factors make it difficult to derive a high accuracy map of the Delta vegetation. In summer, wind speeds are low, flightline edge effects are low, and growth vigor, size of patches, abundance of patches are all high. Hence, the month of August offers the best confluence of ideal imaging conditions, phenological state of invasive plants and the impact of treatment.

8.2 Comparing the Monitoring Scenarios

The Sentinel project has demonstrated that Sentinel imagery can be classified with reasonable accuracy into the same classes that the hyperspectral imagery has been targeting. However, that does not mean that the Sentinel class maps are comparable to the hyperspectral imagery derived maps. The spatial resolution of the two maps is very different with 25 pixels of recent SpecTIR imagery (2x2m) fitting into every single Sentinel pixel (10x10m). This means that there are many more mixed pixels in the images which can only be assigned to a single class, necessarily introducing error in estimating cover and location of invasive species.

A study to determine the feasibility of mapping the Delta (filling the data gap between 2009 and 2013) using fine spatial resolution satellite imagery like WorldView-2, IKONOS, Quickbird, etc. has just been funded. This study will help determine if these sensors can offer us the same maps that Sentinel is able to produce, but at a resolution that the airborne hyperspectral imagery is able to provide. A previous study looking at the impact of oil spills on salt marshes showed that even if these satellite sensors could map the region at the same spatial resolution as airborne hyperspectral, the data quality (Signal-to-noise

ratio) of the hyperspectral imagery was much better allowed a more accurate determination of oil stress (Khanna et al., 2018c). This might also be true of invasive species mapping applications.

Following the arguments laid out in the previous section (8.2), we do not recommend capturing hyperspectral imagery more than once a year. Overall, our recommendation is to use *some combination of scenario 2 (airborne hyperspectral sensor) and 3 (a global satellite sensor like Sentinel-2)* to produce a detailed accurate map of aquatic vegetation in the Delta once a year and use the satellite sensor derived maps to track changes in phenology and plant health seasonally and annually.

8.3 Evaluation of Changing DBW Treatment Plans

We could not conduct this part of the experiment because we were unable to acquire treatment location/date data for 2019 and 2020. The 2019 annual treatment plan report published by DBW did not include appendices with information on type and amount of herbicide applied on a particular date per site in the Delta. The 2020 report has not been published yet. Hence, we could not procure this information and could not evaluate how the change in target species and timing of application has affected treatment efficacy.

8.4 Google Earth Engine Applications for Sentinel Project

The development of Google Earth Engine (GEE) application and scripts will be shared within the Sentinel project report since this GEE deliverable is more closely related to that project.

9. Site Maps

This section contains maps of the seven focus areas showing change from 2004 to 2020. For four sites, we also show the change in mat density for some years.

9.1 Sherman Lake

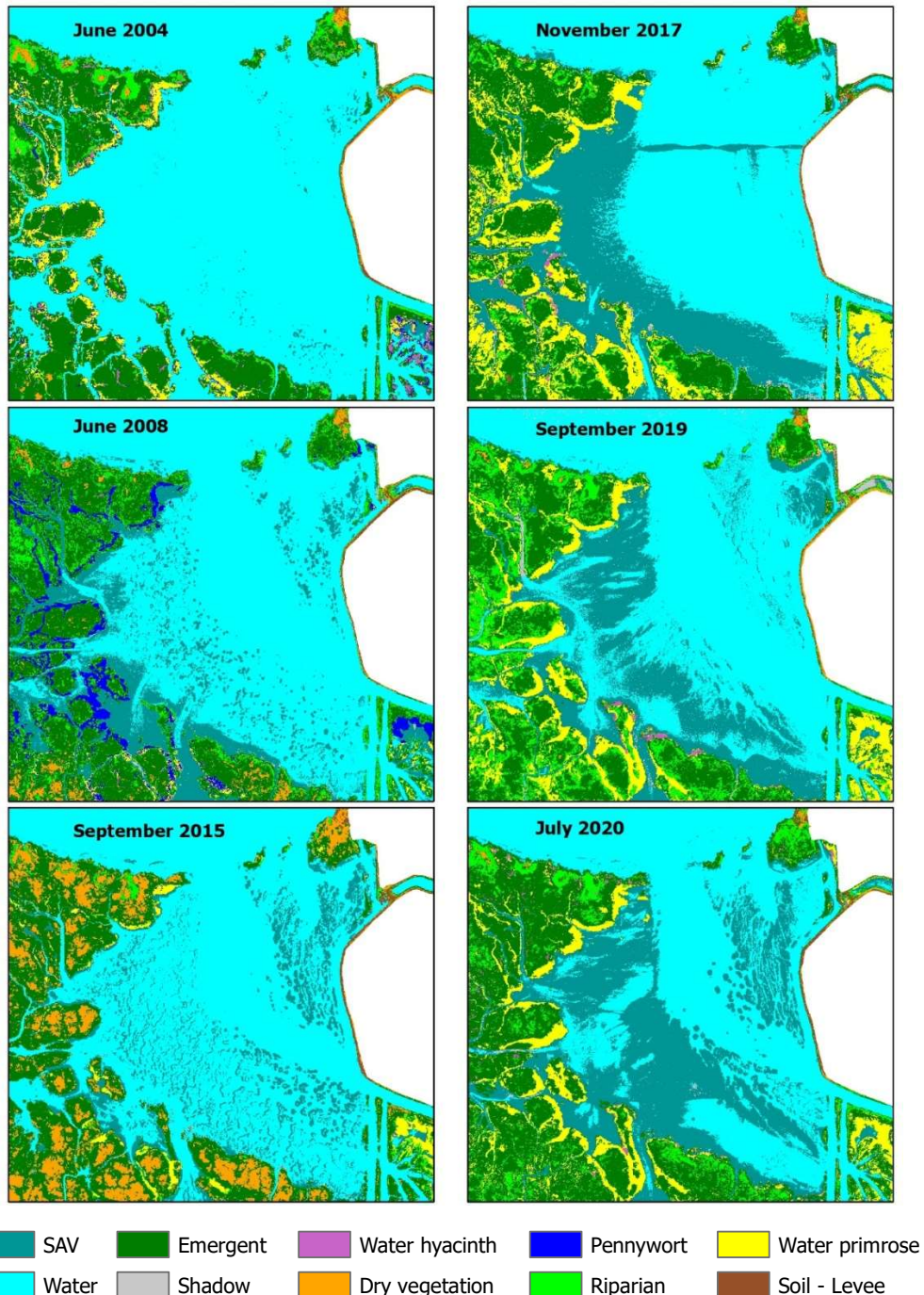


Figure 8-1: Class maps of Sherman Lake in western Delta from 2004 to 2020.

SAV in Sherman Lake has spread and ebbed through the years overall not showing a trend towards increase or decrease in cover (Figure 8-1). The scalloped patterns seen most clearly in 2015 on both the western and eastern sides of the lake (Figures 8-1 & 8-2) are formed by *Stukenia pectinata* patches and tend to spread out in arched patterns. However, in 2020, we see that the eastern patches are getting quite thick and there is a ridge along the middle which probably overlaying a sandbar which shows thick growth of SAV (Figure 8-2). In addition to *S. pectinata*, *E. densa*, *C. demersum*, and *M. spicatum* have also been recorded in Sherman Lake in recent years. Moreover, this year during field work, we discovered a couple of patches of a new invasive SAV species which was first recorded in 2017 in the Delta, *Vallisneria australis* (ribbon weed). Ribbon weed tends to grow very thickly and concentrically out from its starting point making round patches. We found through observations of historical imagery on google earth, that one of the largest patches in Sherman Lake positively identified as ribbon weed this year, has existed in the same spot since 2014, which might be the original entry point of the species.

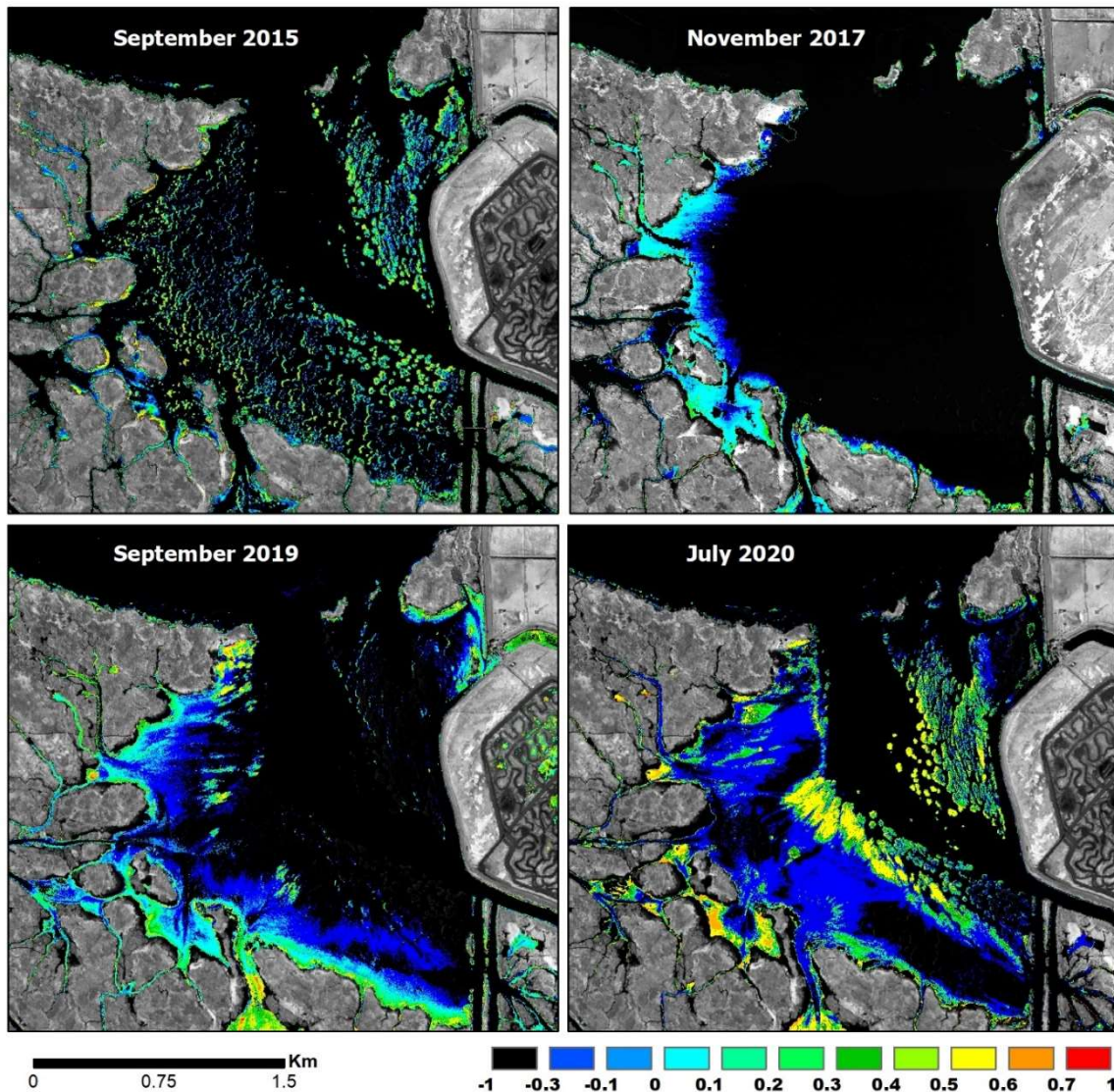


Figure 8-2: SAV mat density in September 2015, October 2018, September 2019 and July 2020 in Sherman Lake.

9.2 Big Break

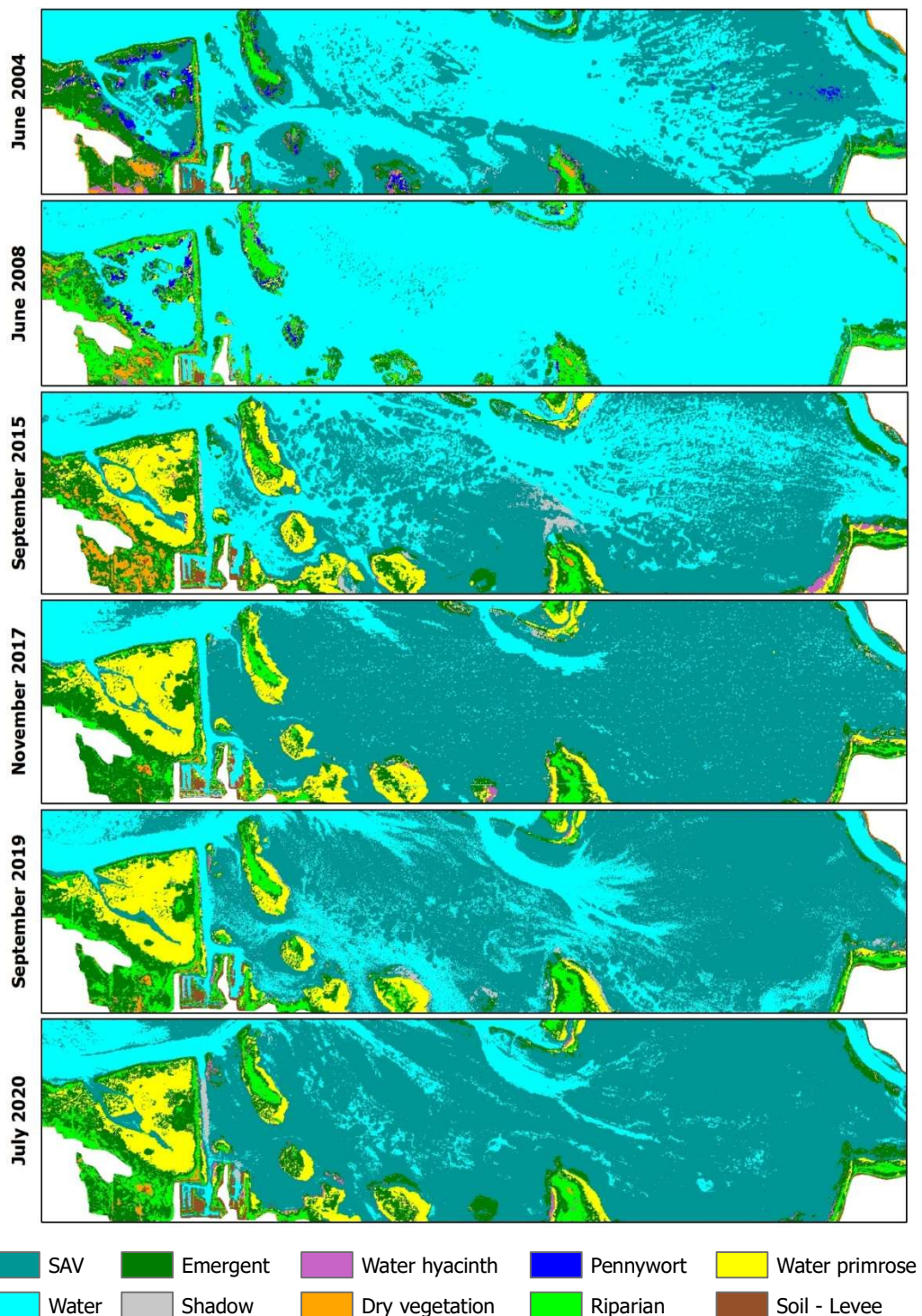


Figure 8-3: Class maps of Big Break in western Delta from 2004 to 2020.

Big Break is slightly east of Sherman Lake but still in the western Delta. The SAV community in Big Break is more diverse co-dominated by *S. pectinata*, *M. spicatum*, *P. crispus*, *C. demersum*, and *E. densa*. Figure 8-3 shows the change in distribution of SAV and FAV from 2015 to 2020. SAV cover has generally

increased over the years, and the central portion of the flooded island in the east end has filled in with SAV compared to the early years. During the 2015 implementation of the drought barrier, the expectation was that Big Break would see a decrease in SAV cover because of increased salinity due to the barrier. However, we observed that SAV cover increased and the species composition changed towards species more tolerant of higher salinities e.g. *S. pectinata* (Kimmerer et al., 2019).

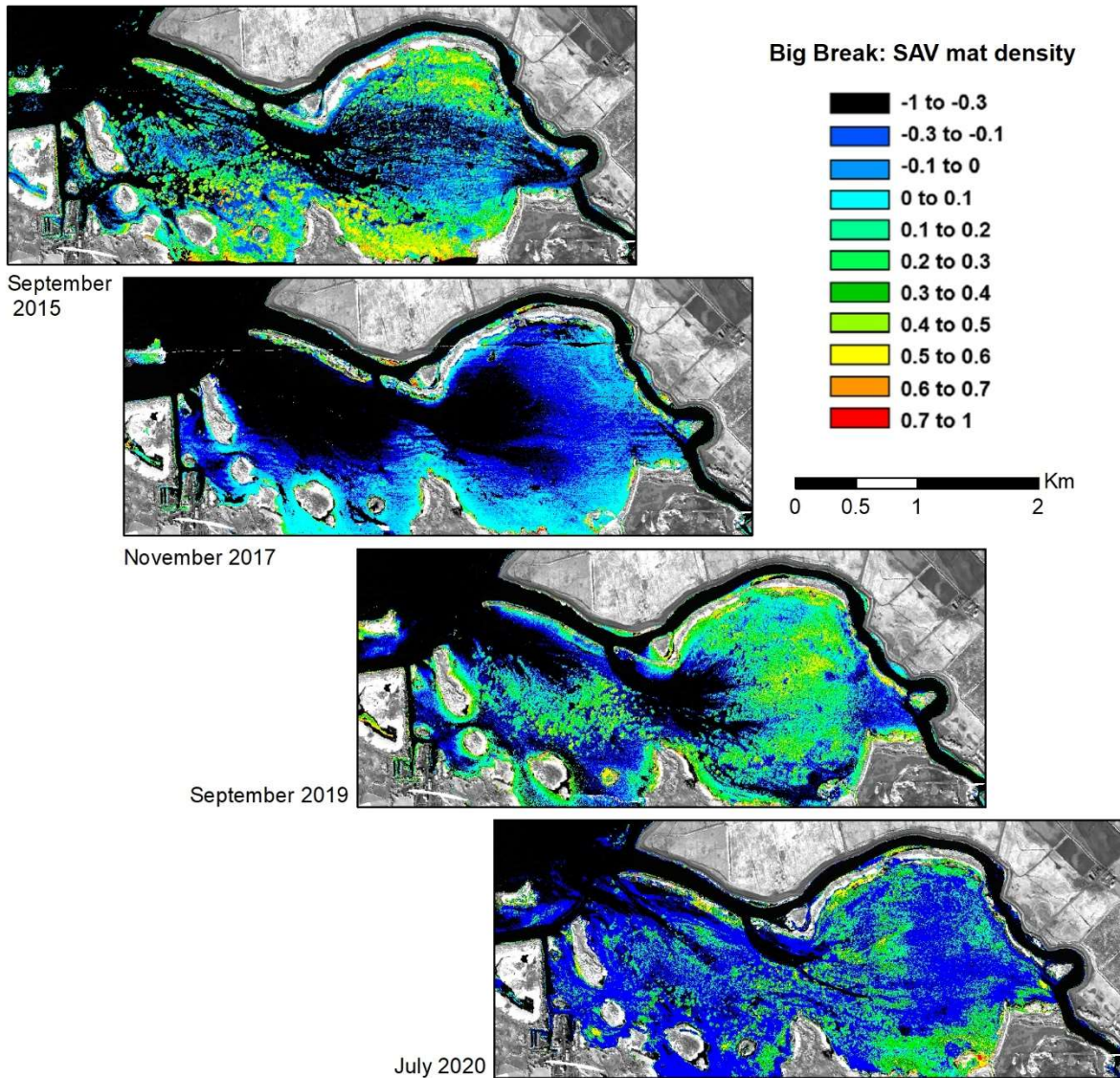


Figure 8-4: SAV mat density from 2015 to 2020 in Big Break.

9.3 Liberty Island

Liberty Island flooded in 1998 due to a levee breach and since then has been a natural experiment in wetland expansion. In the early period (2004-2008), emergent wetland area increased in cover each year. In those years, coarse substrate underlying this large shallow island and wind generated wave action prevented the establishment of SAV in Liberty Island. But, in recent years, two major changes

have happened in this region. Water primrose has increased in cover filling up the narrow regions between marsh patches and then infiltrating into the marsh (Khanna et al., 2018b).

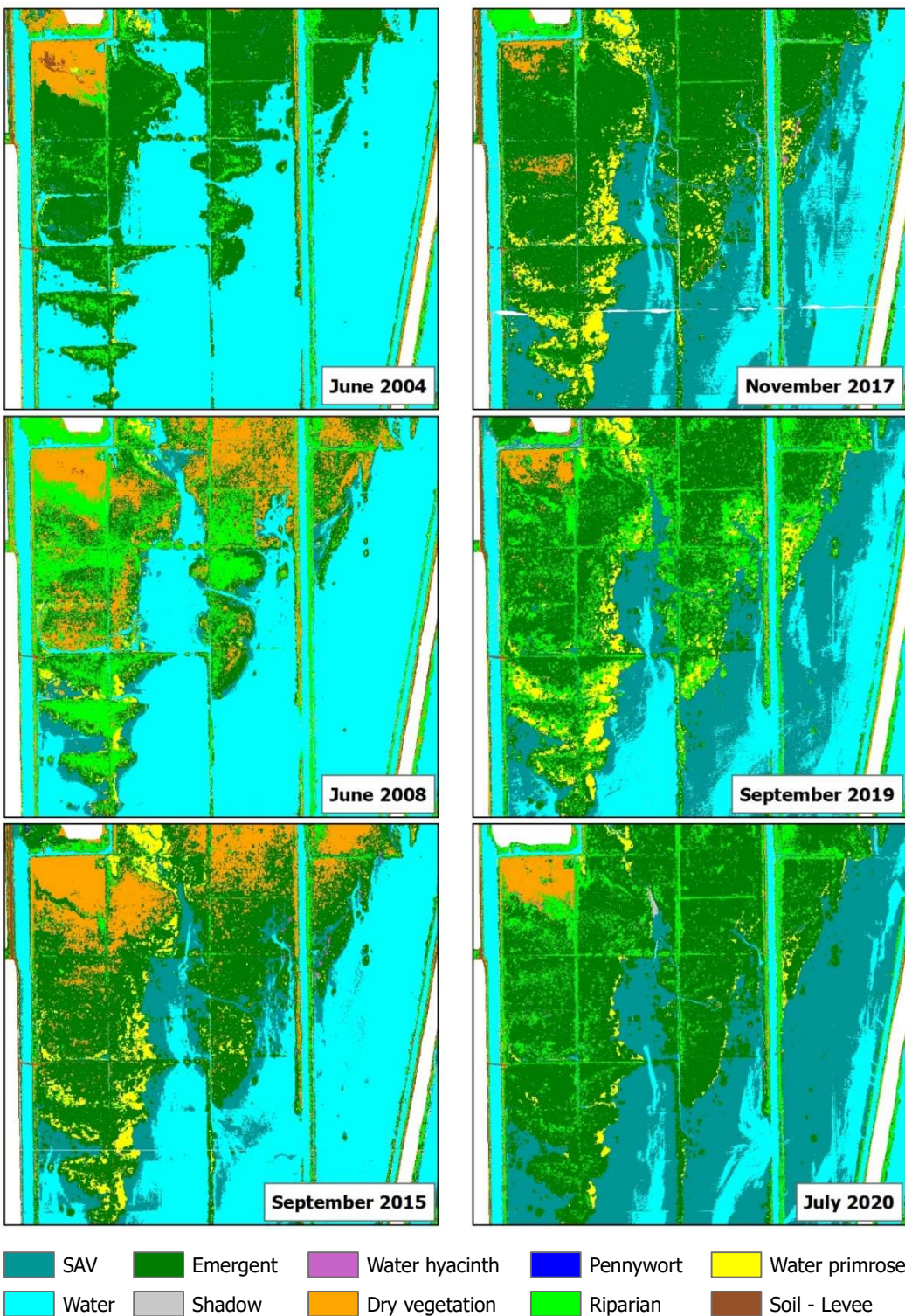


Figure 8-5: Class maps of the northwestern end of Liberty Island from 2004-2020. Note the encroachment of water primrose into emergent marshes. The marsh dryness varies across years (note variable NPV cover across years).

During the recent drought, SAV has also increased in the northern region of the island likely dampening wind-driven wave action and causing fine sediment to deposit in the region. All of these changes are likely fueling a positive feedback for SAV establishment leading to further expansion of SAV (Figure 8-5).

9.4 Frank's Tract

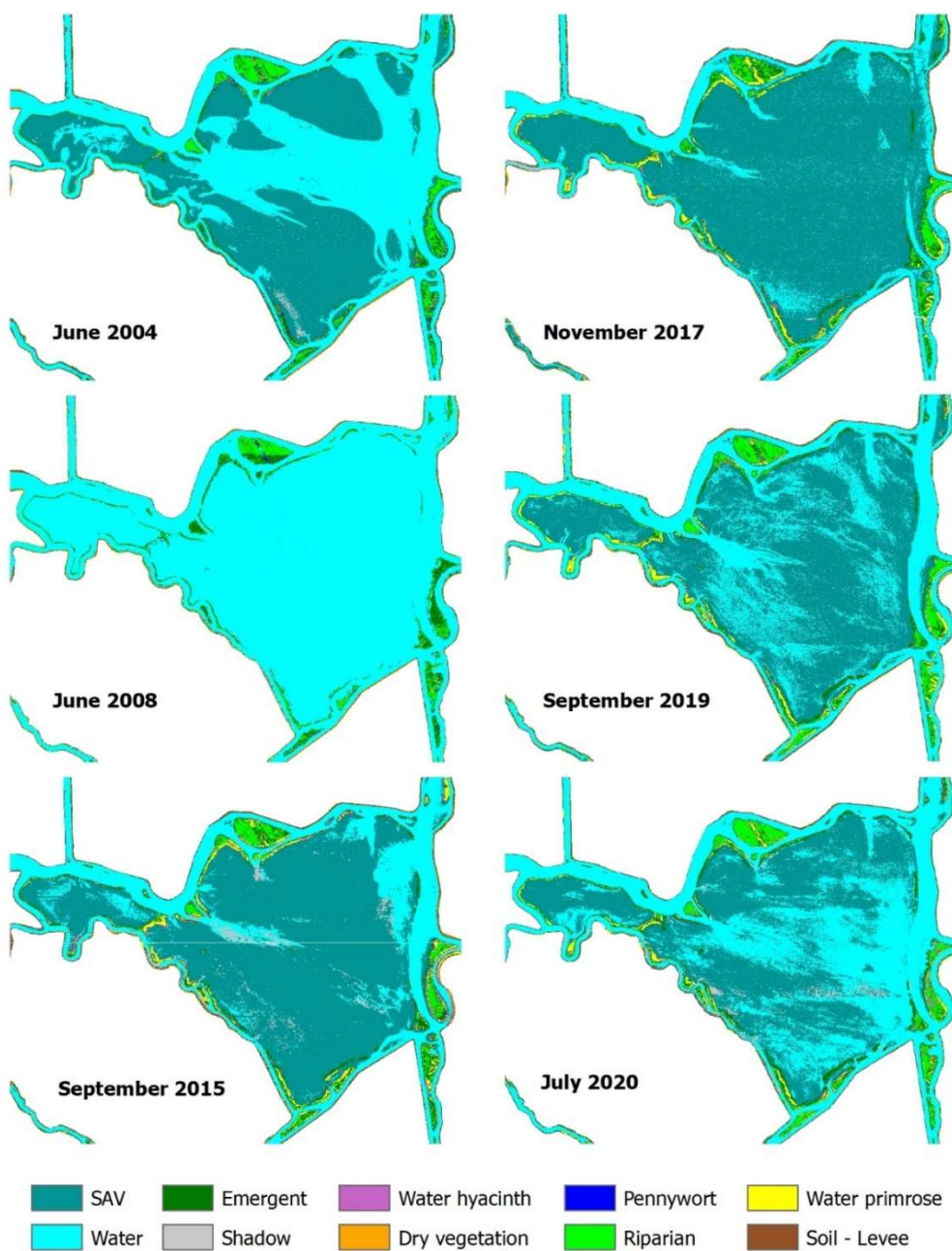


Figure 8-6: Class maps of Frank's Tract from 2004-2020.

In Franks Tract, the SAV community has changed from an *E. densa* dominated community to a more mixed native species dominated community (Caudill et al., 2019). Native SAV canopies are more open and less dense than invasive canopies hence harder to map through remote sensing. In Figure 8-6, we

see that the SAV extent was the greatest in 2015 to 2017, but has reduced somewhat since then. However, Franks Tract is a good example of how tidal stage, rough water surface, and flightline effects can affect SAV classification. High tide and turbid waters can cause the SAV signal to be suppressed e.g. in 2020. Flightline edge effects show up as abrupt changes in SAV cover at the upper or lower edge of the flightline (noticeable in 2019 and 2020). Under these confounding conditions, density calculations are also less reliable hence we don't show them here.

9.5 Rhode Island

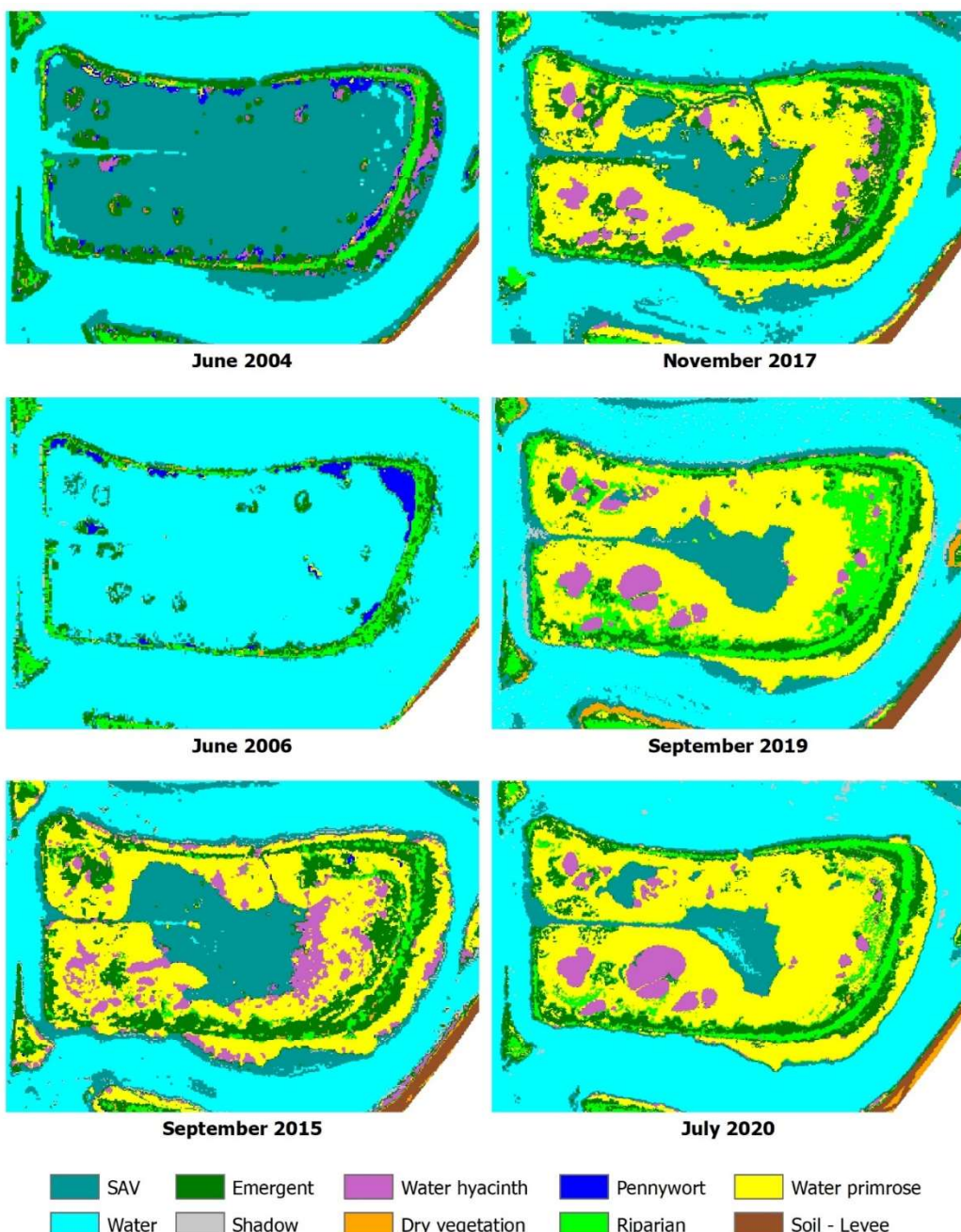


Figure 8-7: Class maps for Rhode Island from 2004-2020.

Rhode Island was flooded in 1938, and between 2004 and 2020, saw a major shift from submerged to a floating aquatic community (Figure 8-7). During the early period, the flooded island was dominated by SAV cover and there were scattered water hyacinth and pennywort mats at the edges. But in recent years, almost the entire island has filled in with water primrose with scattered water hyacinth mats in a few places. This change has stayed pretty consistent since 2017 (Figure 8-7).

9.6 Venice Cut

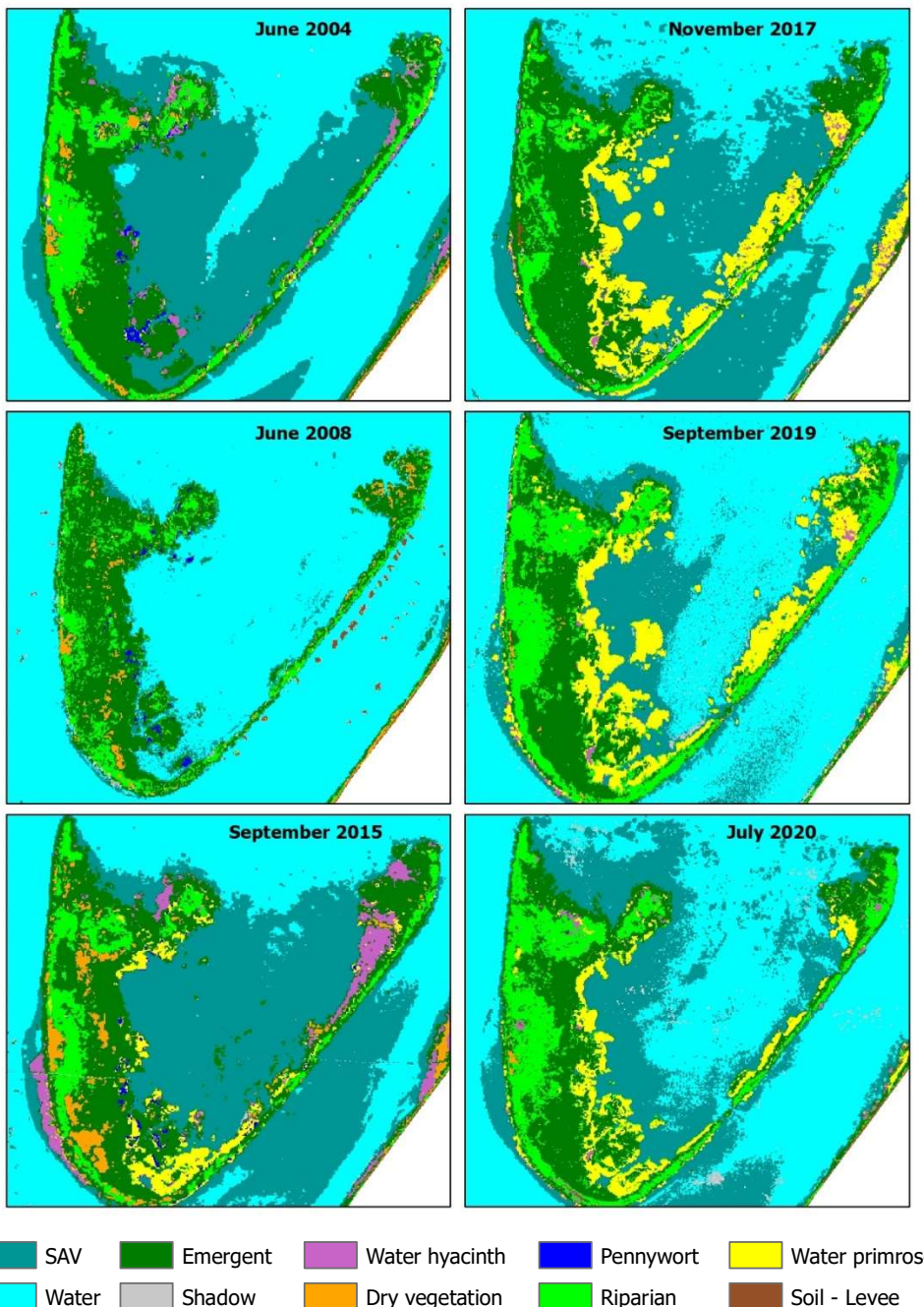


Figure 8-8 SAV and FAV cover in Venice Cut from 2004 - 2020

The main change in Venice Cut has been the increase of both water primrose mats along the inside edge of the island and an increase in pure *Cabomba caroliniana* mats in the southern end of the island. We have also observed water primrose infiltration into the emergent marsh patches of this island, especially in the northwest edge of the island.

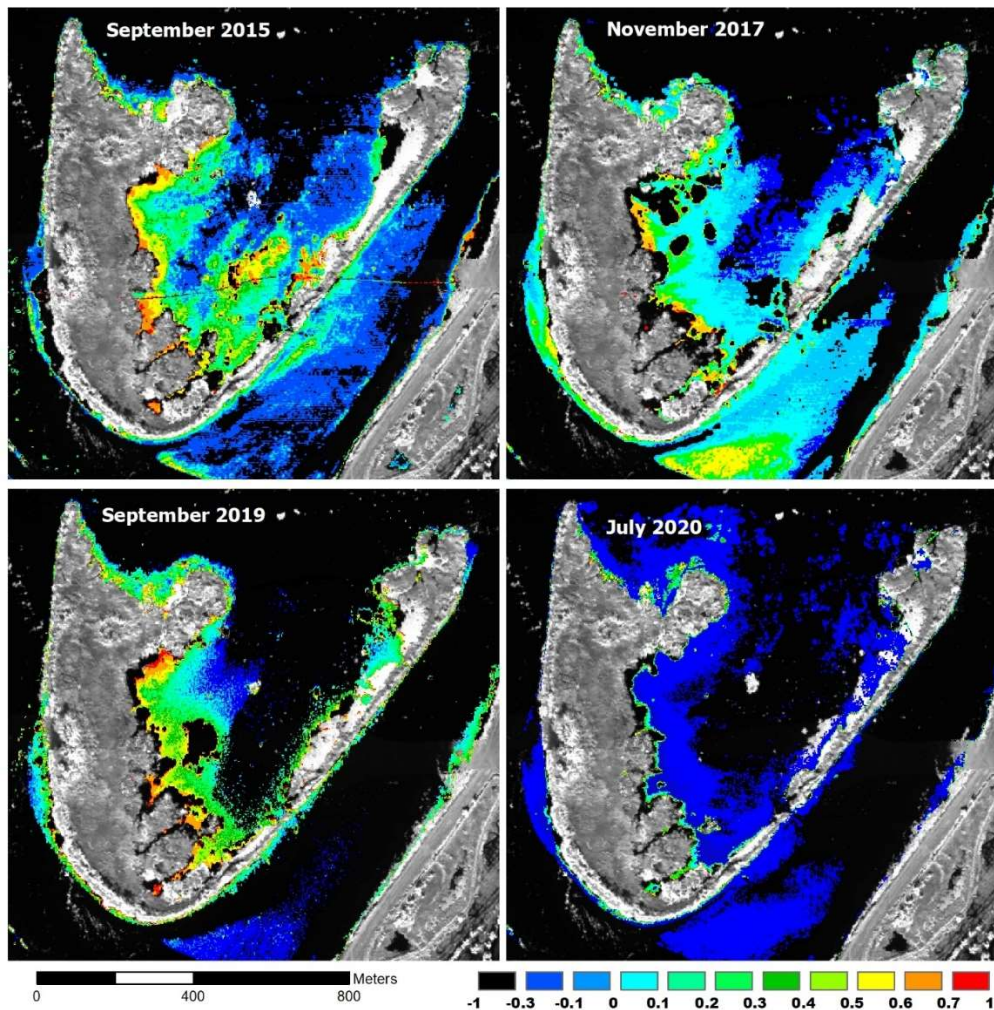


Figure 8-9: SAV mat density in Venice cut from 2015-2020.

9.7 Ward Cut

In Ward Cut, the dominant change from early years is a replacement from pennywort and water hyacinth mats to water primrose and water hyacinth. SAV has been mostly constant within the flooded island pair.

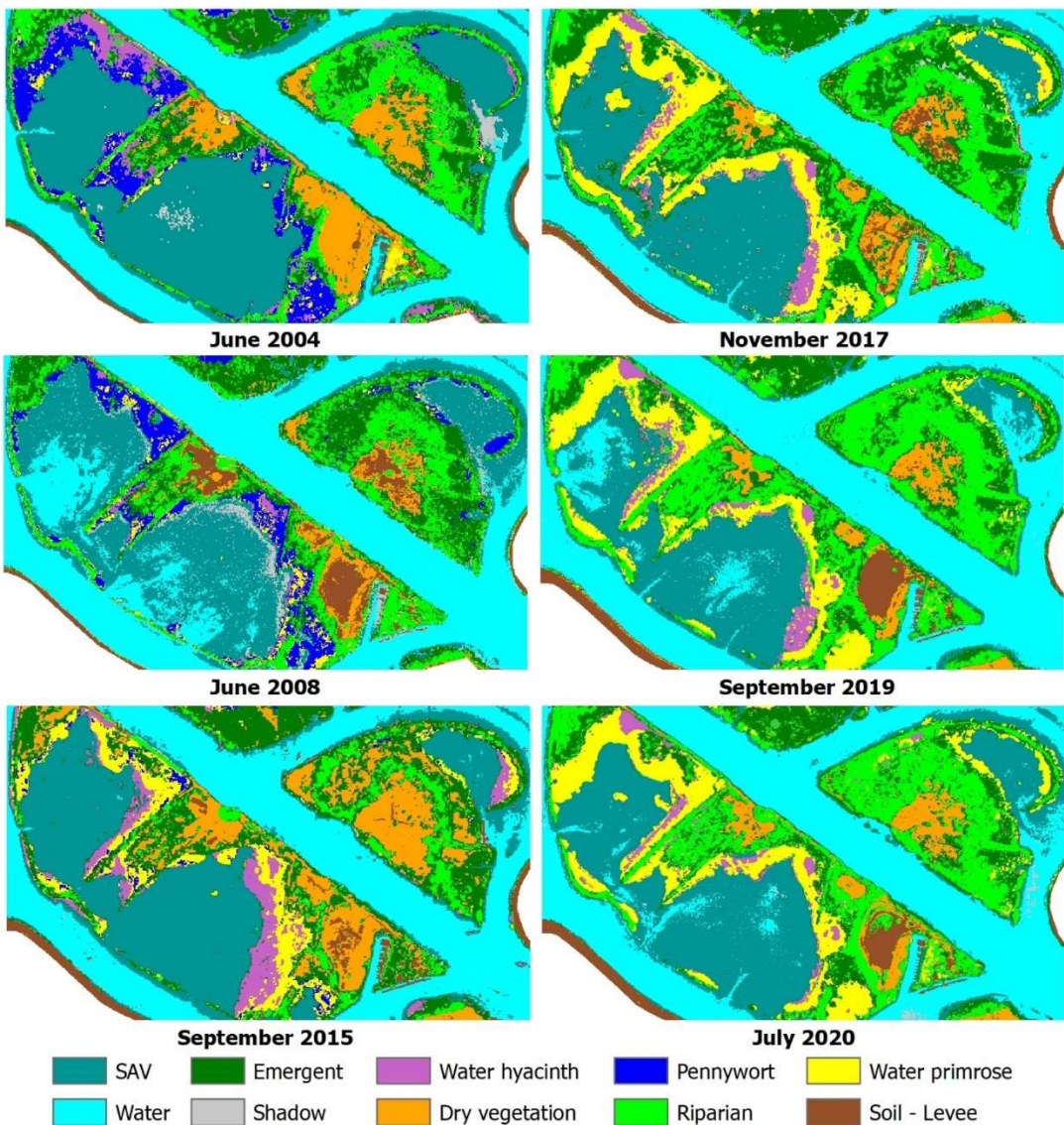


Figure 8-10: Class maps of Ward Cut from 2004-2020.

10. References

- Ackleson, S.G., Klemas, V., 1987. Remote sensing of submerged aquatic vegetation in lower Chesapeake bay: A comparison of Landsat MSS to TM imagery. *Remote Sensing of Environment* 22, 235–248.
- Adams, J.B., Sabol, D.E., Kapos, V., Almeida Filho, R., Roberts, D.A., Smith, M.O., Gillespie, A.R., 1995. Classification of multispectral images based on fractions of endmembers: Application to land-cover change in the Brazilian Amazon. *Remote Sensing of Environment* 52, 137–154. [https://doi.org/doi:10.1016/0034-4257\(94\)00098-8](https://doi.org/doi:10.1016/0034-4257(94)00098-8)
- Alberotanza, L., 1999. Hyperspectral aerial images. A valuable tool for submerged vegetation recognition in the Orbetello Lagoons, Italy. *International Journal of Remote Sensing* 20, 523–533.
- Bicudo, D.D.C., Fonseca, Bár.M., Bini, L.M., Crossetti, L.O., Bicudo, C.E.D.M., AraÚJo-Jesus, T., 2007. Undesirable side-effects of water hyacinth control in a shallow tropical reservoir. *Freshwater Biology* 52, 1120–1133. <https://doi.org/10.1111/j.1365-2427.2007.01738.x>
- Bossard, C.C., Randall, J.M., Hoshovsky, M.C., 2000. Invasive plants of California's wildlands. University of California Press, Berkeley.
- Breiman, L., 2001. Random Forests. *Machine Learning* 45, 5–32. <https://doi.org/10.1023/a:1010933404324>
- Cal-IPC, 2006. California Invasive Plant Inventory. Cal-IPC Publication, Berkeley, California.
- Caudill, J., Jones, A.R., Anderson, L., Madsen, J.D., Gilbert, P., Shuler, S., Heilman, M.A., 2019. Aquatic plant community restoration following the long-term management of invasive *Egeria densa* with fluridone treatments. *Management of Biological Invasions* 10, 473–485. <https://doi.org/10.3391/mbi.2019.10.3.05>
- Clark, R.N., Roush, T.L., 1984. Reflectance spectroscopy - Quantitative analysis techniques for remote sensing applications. *Journal of Geophysical Research Solid Earth* 89, 6329–6340. <https://doi.org/doi:10.1029/JB089iB07p06329>
- Cohen, A.N., Carlton, J.T., 1998. Accelerating Invasion Rate in a Highly Invaded Estuary. *Science* 279, 555–558. <https://doi.org/doi:10.1126/science.279.5350.555>
- Cook, C.D.K., 1990. Aquatic plant book. SPB Academic Pub., The Hague, The Netherlands.
- Cook, C.D.K., Urmi-König, K., 1984. A Revision of the Genus *Egeria* (Hydrocharitaceae). *Aquatic Botany* 19, 73–96.
- DBW, 2018. Submersed Aquatic Vegetation Control Program [Egeria densa, Curlyleaf Pondweed, Eurasian Watermilfoil, Fanwort, and Coontail]. Sacramento, CA, USA.
- El-Gendy, A.S., Biswas, N., Bewtra, J.K., 2005. A floating aquatic system employing water hyacinth for municipal landfill leachate treatment: effect of leachate characteristics on the plant growth. *Journal of Environmental Engineering and Science* 4, 227–240. <https://doi.org/10.1139/s04-053>
- Gamon, J.A., Field, C.B., Bilger, W., Björkman, O., Fredeen, A.L., Peñuelas, J., 1990. Remote sensing of the xanthophyll cycle and chlorophyll fluorescence in sunflower leaves and canopies. *Oecologia* 85, 1–7.
- Gamon, J.A., Surfus, J.S., 1999. Assessing leaf pigment content and activity with a reflectometer. *New Phytologist* 143, 105–117.
- Gitelson, A., Merzlyak, M.N., 1994. Spectral reflectance changes associated with autumn senescence of *Aesculus-hippocastanum* L. and *Acer-platanoides* L. leaves - Spectral features and relation to chlorophyll estimation. *Journal of Plant Physiology* 143, 286–292.
- Gitelson, A.A., Merzlyak, M.N., Chivkunova, O.B., 2001. Optical properties and nondestructive estimation of anthocyanin content in plant leaves. *Photochemistry and Photobiology* 74, 38–45.

- Gitelson, A.A., Merzlyak, M.N., Lichtenthaler, H.K., 1996. Detection of red edge position and chlorophyll content by reflectance measurements near 700 nm. *Journal of Plant Physiology* 148, 501–508.
- Gitelson, A.A., Zur, Y., Chivkunova, O.B., Merzlyak, M.N., 2002. Assessing carotenoid content in plant leaves with reflectance spectroscopy. *Photochemistry and Photobiology* 75, 272–281.
- Gopal, B., 1987. Water hyacinth, Aquatic plant studies I. Elsevier, Amsterdam, the Netherlands.
- Hestir, E.L., 2010. Trends in estuarine water quality and submerged aquatic vegetation invasion. Geography. University of California, Davis.
- Hestir, E.L., Khanna, S., Andrew, M.E., Santos, M.J., Viers, J.H., Greenberg, J.A., Rajapakse, S.S., Ustin, S.L., 2008. Identification of invasive vegetation using hyperspectral remote sensing in the California Delta ecosystem. *Remote Sensing of Environment* 112. <https://doi.org/10.1016/j.rse.2008.01.022>
- Hirano, A., Madden, M., Welch, R., 2003. Hyperspectral image data for mapping wetland vegetation. *Wetlands* 23, 436–448. <https://doi.org/doi:10.1672/18-20>
- Horppila, J., Nurminen, L., 2003. Effects of submerged macrophytes on sediment resuspension and internal phosphorus loading in Lake Hiidenvesi (southern Finland). *Water Research* 37, 4468–4474. [https://doi.org/10.1016/s0043-1354\(03\)00405-6](https://doi.org/10.1016/s0043-1354(03)00405-6)
- Huete, A.R., 1986. Separation of soil-plant spectral mixtures by factor analysis. *Remote Sensing of Environment* 19, 237–251. [https://doi.org/http://dx.doi.org/10.1016/0034-4257\(86\)90055-6](https://doi.org/http://dx.doi.org/10.1016/0034-4257(86)90055-6)
- Hunt, E.R., Rock, B.N., 1989. Detection of changes in leaf water content using near-infrared and middle-infrared reflectances. *Remote Sensing of Environment* 30, 43–54.
- Khanna, S., Conrad, J.L., Caudill, J., Christman, M., Darin, G., Ellis, D., Gilbert, P., Hartman, R., Kayfetz, K., Pratt, W., Tobias, V., Wasserman, A., 2018a. Framework for Aquatic Vegetation Monitoring in the Delta. Aquatic Vegetation Project Work Team, Interagency Ecological Program.
- Khanna, S., Palacios-Orueta, A., Whiting, M.L., Ustin, S.L., Riaño, D., Litago, J., 2007. Development of angle indexes for soil moisture estimation, dry matter detection and land-cover discrimination. *Remote Sensing of Environment* 109. <https://doi.org/10.1016/j.rse.2006.12.018>
- Khanna, S., Santos, M.J., Boyer, J.D., Shapiro, K.D., Bellvert, J., Ustin, S.L., 2018b. Water primrose invasion changes successional pathways in an estuarine ecosystem. *Ecosphere* 9, e02418. <https://doi.org/https://doi.org/10.1002/ecs2.2418>
- Khanna, S., Santos, M.J., Ustin, S.L., Haverkamp, P.J., 2011. An integrated approach to a biophysically based classification of floating aquatic macrophytes. *International Journal of Remote Sensing* 32. <https://doi.org/10.1080/01431160903505328>
- Khanna, S., Santos, M.J., Ustin, S.L., Koltunov, A., Kokaly, R.F., Roberts, D.A., 2013. Detection of salt marsh vegetation stress and recovery after the Deepwater Horizon Oil Spill in Barataria Bay, Gulf of Mexico using AVIRIS data. *PLoS ONE* 8. <https://doi.org/10.1371/journal.pone.0078989>
- Khanna, S., Santos, M.J., Ustin, S.L., Shapiro, K.D., Haverkamp, P.J., Lay, M., 2018c. Comparing the potential of multispectral and hyperspectral data for monitoring oil spill impact. *Sensors (Switzerland)* 18. <https://doi.org/10.3390/s18020558>
- Kimmerer, W., Wilkerson, F., Downing, B., Dugdale, R., Gross, E.S., Kayfetz, K., Khanna, S., Parker, A.E., Thompson, J., 2019. Effects of drought and the emergency drought barrier on the ecosystem of the California Delta. *San Francisco Estuary and Watershed Science* 17, Article 2. <https://doi.org/https://doi.org/10.15447/sfews.2019v17iss3art1>
- Koch, E., 2001. Beyond light: Physical, geological, and geochemical parameters as possible submersed aquatic vegetation habitat requirements. *Estuaries and Coasts* 24, 1–17. <https://doi.org/10.2307/1352808>
- Kruse, F.A., Lefkoff, A.B., Boardman, J.W., Heidebrecht, K.B., Shapiro, A.T., Barloon, P.J., Goetz, A.F.H., 1993. The spectral image processing system (SIPS)-interactive visualization and analysis of imaging

- spectrometer data. *Remote Sensing of Environment* 44, 145–163. <https://doi.org/doi:10.1063/1.44433>
- Lacy, J.R., Foster-Martinez, M.R., Allen, R.M., Drexler, J.Z., 2021. Influence of invasive submerged aquatic vegetation (*E. densa*) on currents and sediment transport in a freshwater tidal system. *Water Resources Research* 57, e2020WR028789. <https://doi.org/https://doi.org/10.1029/2020WR028789>
- Lehmann, A., Lachavanne, J.-B.B., 1997. Geographic information systems and remote sensing in aquatic botany. *Aquatic Botany* 58, 195–207.
- Lillesand, T.M., Kiefer, R.W., Chipman, J.W., 2004. *Remote Sensing and Image Interpretation*. John Wiley & Sons, Inc., New York, NY, USA.
- Merenyi, E., Farrand, W.H., Stevens, L.E., Melis, T.S., Chhibber, K., 2000. Studying the potential for monitoring Colorado River ecosystem resources below Glen Canyon Dam using low-altitude AVIRIS data, in: 9th AVIRIS Earth Science and Applications Workshop. Pasadena, CA.
- Motohka, T., Nasahara, K.N., Oguma, H., Tsuchida, S., 2010. Applicability of Green-Red Vegetation Index for Remote Sensing of Vegetation Phenology. *Remote Sensing* 2, 2369–2387. <https://doi.org/10.3390/rs2102369>
- Nagler, P.L., Daughtry, C.S.T., Goward, S.N., 2000. Plant litter and soil reflectance. *Remote Sensing of Environment* 71, 207–215. [https://doi.org/doi:10.1016/S0034-4257\(99\)00082-6](https://doi.org/doi:10.1016/S0034-4257(99)00082-6)
- Nichols, F.H., Cloern, J.E., Luoma, S.N., Peterson, D.H., 1986. The Modification of an Estuary. *Science* 231, 567–573. <https://doi.org/10.1126/science.231.4738.567>
- Penfound, W.T., Earle, T.T., 1948. The Biology of Water Hyacinth. *Ecological Monographs* 18, 447–472. <https://doi.org/doi:10.2307/1948585>
- Peñuelas, J., Baret, F., Filella, I., 1995. Semi-empirical indices to assess carotenoids/ chlorophyll A ratio from leaf spectral reflectance. *Photosynthetica* 31, 221–230.
- Rejmánková, E., 1992. Ecology of creeping macrophytes with special reference to *Ludwigia peploides* (H.B.K.) Raven. *Aquatic Botany* 43, 283–299. [https://doi.org/doi:10.1016/0304-3770\(92\)90073-R](https://doi.org/doi:10.1016/0304-3770(92)90073-R)
- Rosenfield, G.H., Fitzpatrick-Lins, K., 1986. A coefficient of agreement as a measure of thematic classification accuracy. *Photogrammetric engineering and remote sensing* 52, 223–227.
- Santos, M.J., Anderson, L.W.J., Ustin, S.L., 2010. Effects of invasive species on plant communities: an example using submersed aquatic plants at the regional scale. *Biological Invasions* 13, 443–457. <https://doi.org/10.1007/s10530-010-9840-6>
- Santos, M.J., Hestir, E.L., Khanna, S., Ustin, S.L., 2012. Image spectroscopy and stable isotopes elucidate functional dissimilarity between native and nonnative plant species in the aquatic environment. *New Phytologist* 193. <https://doi.org/10.1111/j.1469-8137.2011.03955.x>
- Santos, M.J., Khanna, S., Hestir, E.L., Andrew, M.E., Rajapakse, S.S., Greenberg, J.A., Anderson, L.W.J., Ustin, S.L., 2009. Use of Hyperspectral Remote Sensing to Evaluate Efficacy of Aquatic Plant Management in the Sacramento-San Joaquin River Delta, California. *Invasive Plant Science and Management* 2, 216–229. <https://doi.org/10.1614/IPSM-08-115.1>
- Sawaya, K.E., Olmanson, L.G., Heinert, N.J., Brezonik, P.L., Bauer, M.E., 2003. Extending satellite remote sensing to local scales: land and water resource monitoring using high-resolution imagery. *Remote Sensing of Environment* 88, 144–156. <https://doi.org/doi:10.1016/j.rse.2003.04.0006>
- Scheffer, M., Szabó, S., Gragnani, A., van Nes, E.H., Rinaldi, S., Kautsky, N., Norberg, J., Roijackers, R.M.M., Franken, R.J.M., 2003. Floating plant dominance as a stable state. *Proceedings of the National Academy of Sciences* 100, 4040–4045. <https://doi.org/10.1073/pnas.0737918100>
- Scheffer, M., van Nes, E.H., Martens, K., 2007. Shallow lakes theory revisited: various alternative regimes driven by climate, nutrients, depth and lake size, in: Gulati, R.D., Lammens, E., Pauw, N., Donk, E. (Eds.), *Shallow Lakes in a Changing World*. Springer Netherlands, pp. 455–466.

https://doi.org/10.1007/978-1-4020-6399-2_41

- Sculthorpe, C.D., 1967. The biology of aquatic vascular plants. Edward Arnold, London.
- Silvestri, S., Marani, M., Marani, A., 2003. Hyperspectral remote sensing of salt marsh vegetation, morphology and soil topography. Physics and Chemistry of the Earth, Parts A/B/C 28, 15–25. [https://doi.org/doi:10.1016/S1474-7065\(03\)00004-4](https://doi.org/doi:10.1016/S1474-7065(03)00004-4)
- Smith, M.O., Ustin, S.L., Adams, J.B., Gillespie, A.R., 1990. Vegetation in deserts: I. A regional measure of abundance from multispectral images. Remote Sensing of Environment 31, 1–26. [https://doi.org/doi:10.1016/0034-4257\(90\)90074-V](https://doi.org/doi:10.1016/0034-4257(90)90074-V)
- Story, M., Congalton, R.G., 1986. Accuracy assessment - A user's perspective (map interpretation). Photogrammetric Engineering and Remote Sensing 52, 397–399.
- Tucker, C.J., 1979. Red and photographic infrared linear combinations for monitoring vegetation. Remote Sensing of Environment 8, 127–150. [https://doi.org/doi:10.1016/0034-4257\(79\)90013-0](https://doi.org/doi:10.1016/0034-4257(79)90013-0)
- Ward, D.H., Morton, A., Tibbitts, T.L., Douglas, D.C., Carrera-Gonzalez, E., 2003. Long-term change in eelgrass distribution at Bahia San Quintin, Baja California, Mexico, using satellite imagery. Estuaries 26, 1529–1539.
- Wilcock, R.J., Champion, P.D., Nagels, J.W., Croker, G.F., 1999. The influence of aquatic macrophytes on the hydraulic and physico-chemical properties of a New Zealand lowland stream. Hydrobiologia 416, 203–214. <https://doi.org/10.1023/a:1003837231848>
- Wright, S.A., Schoellhamer, D.H., 2004. Trends in the Sediment Yield of the Sacramento River, California, 1957 – 2001. San Francisco Estuary and Watershed Science 2, article 2.
- Zhang, X., 1998. On the estimation of biomass of submerged vegetation using Landsat thematic mapper (TM) imagery: a case study of the Honghu Lake, PR China. International Journal of Remote Sensing 19, 11–20.

11. Appendix A. Classifier inputs and their description

Acronym	Description
Indices	Index inputs
NDVI	Normalized Difference Vegetation Index (<i>Leaf area and pigment indicator</i>)
gNDVI	Green NDVI (<i>Pigment indicator</i>)
mNDVI	Modified (or Red-Edge) NDVI (<i>Leaf area and pigment indicator</i>)
RG_Ratio	Red-Green Ratio (<i>Anthocyanin indicator</i>)
NDII	Normalized Difference Infrared Index (<i>Indicator of canopy water content</i>)
NDII2	NDII using SWIR band at ~2200 nm (<i>Indicator of canopy water content</i>)
LPI	Leaf Pigment Index (<i>Pigment indicator</i>)
ANIR	Angle at NIR (<i>Tracks changes in plant condition, e.g. the transition between live and senescent vegetation</i>)
ARed	Angle at Red (<i>Tracks changes in plant condition</i>)
ASWIR1	Angle at SWIR1 (or ~1600 nm) (<i>Indicator of canopy and soil water content</i>)
GI	Green Index (<i>Phenology indicator</i>)
PRI	Photochemical Reflectance Index (<i>Indicator of photosynthesis</i>)
CAI	Cellulose Absorption Index (<i>Cellulose indicator</i>)
WADI	Water Absorption Difference Index for the 1160 nm absorption feature
ADW1	Absorption Depth of Water at 990 nm
ADW2	Absorption Depth of Water at 1170 nm
SICI	Structure Insensitive Pigment Index (<i>Carotenoid and Chlorophyll A indicator</i>)
CRI_550	Carotenoid Reflectance Index using 550 nm band (<i>Carotenoid indicator</i>)
CRI_700	Carotenoid Reflectance Index using 700 nm band (<i>Carotenoid indicator</i>)
ARI	Anthocyanin Reflectance Index (<i>Anthocyanin indicator</i>)
Blue	Reflectance at Blue band
Green	Reflectance at Green band
Red	Reflectance at Red band
NIR	Reflectance at NIR band
SWIR1	Reflectance at SWIR ~1600 nm band
SWIR2	Reflectance at SWIR ~2200 nm band
CRWAT1	Continuum Removal over water absorption at 980 nm (continuum removal explained below)
CRWAT2	Continuum Removal over water absorption at 1160 nm

CRCELL	Continuum Removal over cellulose absorption
SAM inputs	Spectral Angle Mapper
SAM_SAV	SAM band for Submerged Aquatic Vegetation (SAV)
SAM_WH	SAM band for Water Hyacinth
SAM_TULE	SAM band for Tule
SAM_PRIM	SAM band for Water Primrose
SAM_PHRAG	SAM band for Phragmites
SAM_PEN	SAM band for Pennywort
SAM_CAT	SAM band for Cattails
SAM_AZLDK	SAM band for Azolla and Duckweed
SAM_ARND	SAM band for Arundo
SAM_MFL	SAM band for Watermilfoil
SAM_TWAT	SAM band for Turbid Water
SAM_SAGO	SAM band for Sago Pondweed
SAM_ELOD	SAM band for Elodea
SAM_EGER	SAM band for <i>Egeria</i>
SAM_CRLF	SAM band for Curlyleaf pondweed
SAM_COON	SAM band for Coontail
SAM_CWAT	SAM band for Clear Water
SAM_CAB	SAM band for Cabomba
SAM_ALG	SAM band for Algae mats
SMA inputs	Spectral Mixture Analysis
SMA_WAT	SMA percent pixel cover of water
SMA_SOIL	SMA percent pixel cover of soil
SMA_NPV	SMA percent pixel cover of non-photosynthetic vegetation (NPV)
SMA_SAV	SMA percent pixel cover of submerged aquatic vegetation
SMA_FLT	SMA percent pixel cover of floating green vegetation
SMA_EME	SMA percent pixel cover of emergent vegetation
SMA_RMSE	SMA root mean square error
SVIS	SAV Vegetation Index using SAV line